PLOS ONE

RESEARCH ARTICLE

Perturbation of BRMS1 interactome reveals pathways that impact metastasis

Rosalyn C. Zimmermann[1☯], Mihaela E. Sardiu[2,3,4☯*], Christa A. Manton[1,5,6☯], Md. Sayem Miah[2,7☯], Charles A. S. Banks[2], Mark K. Adams[2], Devin C. Koestler[3,4], Douglas R. Hurst[5], Mick D. Edmonds[8], Michael P. Washburn[1,2,4], Danny R. Welch[1,4*]

1 Department of Cancer Biology, The Kansas University Medical Center, Kansas City, KS, United States of America, **2** Stowers Institute for Medical Research, Kansas City, Missouri, United States of America, **3** Department of Biostatistics and Data Science, The Kansas University Medical Center, Kansas City, KS, United States of America, **4** The University of Kansas Cancer Center, Kansas City, KS, United States of America, **5** Pathology Department, University of Alabama at Birmingham, Birmingham, Alabama, United States of America, **6** Department of Biology, Baker University, Baldwin City, KS, United States of America, **7** Department of Biochemistry and Molecular Biology, University of Arkansas for Health Sciences, Little Rock, AR, United States of America, **8** Department of Genetics, University of Alabama at Birmingham, Birmingham, Alabama, United States of America

☯ These authors contributed equally to this work.
* dwelch@kumc.edu (DRW); msardiu@kumc.edu (MES)

Citation: Zimmermann RC, Sardiu ME, Manton CA, Miah M.S, Banks CAS, Adams MK, et al. (2021) Perturbation of BRMS1 interactome reveals pathways that impact metastasis. PLoS ONE 16(11): e0259128. https://doi.org/10.1371/journal.pone.0259128

Editor: Srikumar Chellappan, H. Lee Moffitt Cancer Center & Research Institute, UNITED STATES

Received: July 26, 2021

Accepted: October 12, 2021

Published: November 17, 2021

Data Availability Statement: The mass spectrometry datasets generated for this study are available from the Massive data repository (https://massive.ucsd.edu) using the identifiers listed in S5 Table. For data generated at the Stowers Institute, links to the original data underlying this manuscript can be accessed from the Stowers Original Data Repository at http://www.stowers.org/research/publications/libpb-1585.

Funding: This work was supported by the Stowers Institute for Medical Research (MPW, MES, MSM,

Abstract

Breast Cancer Metastasis Suppressor 1 (BRMS1) expression is associated with longer patient survival in multiple cancer types. Understanding BRMS1 functionality will provide insights into both mechanism of action and will enhance potential therapeutic development. In this study, we confirmed that the C-terminus of BRMS1 is critical for metastasis suppression and hypothesized that critical protein interactions in this region would explain its function. Phosphorylation status at S237 regulates BRMS1 protein interactions related to a variety of biological processes, phenotypes [cell cycle (e.g., CDKN2A), DNA repair (e.g., BRCA1)], and metastasis [(e.g., TCF2 and POLE2)]. Presence of S237 also directly decreased MDA-MB-231 breast carcinoma migration *in vitro* and metastases *in vivo*. The results add significantly to our understanding of how BRMS1 interactions with Sin3/HDAC complexes regulate metastasis and expand insights into BRMS1's molecular role, as they demonstrate BRMS1 C-terminus involvement in distinct protein-protein interactions.

Introduction

Metastasis is a multi-step process that occurs when cells disseminate from the primary neoplasm and eventually colonize distant organs. Successful completion of this complex cascade is associated with nearly all cancer-related morbidities and mortalities. Despite its causative role in cancer-specific mortality and morbidity, a complete understanding of the process and its mechanisms remain elusive. Metastasis is regulated by three types of genes: metastasis-promoting, -suppressing, and -efficiency modifying [1]. The protein of interest in this study, Breast Cancer Metastasis Suppressor 1 (BRMS1), is a metastasis suppressor, which is defined by the ability to suppress metastasis without blocking primary tumor growth [2]. Metastasis

CAB, MKA); METAvivor Research and Support Inc. (DRW), National Institute for General Medical Sciences [GM112639, F32GM122215 (MPW)]; National Foundation for Cancer Research (DRW), USPHS National Cancer Institute [CA134981, CA168524 (DRW)]; American Cancer Society [PF-16-227-01-CSM (CAM)]; Susan G. Komen for the Cure [SAC110037 (DRW)]; The K-INBRE Bioinformatics Core supported in part by the National Institute of General Medical Science [P20-GM103418 (RCZ]; the KU Cancer Center Biostatistics and Informatics Shared Resource supported by the National Cancer Institute Cancer Center [P30-CA168524 (DK, DRW)]; and the Kansas Institute for Precision Medicine COBRE supported by the National Institute of General Medical Science [P20-GM130423 (DCK)]. The funders had no role in study design, data collection and analysis, decision to publish, or preparation of the manuscript.

Competing interests: The authors have declared that no competing interests exist.

suppressors are of distinct interest because, by preventing the successful completion of the metastatic cascade, the devastating sequalae or deaths associated with metastasis are inhibited [3, 4].

BRMS1 was discovered in the year 2000 and its re-expression in multiple cell lines significantly decreases lung metastases in syngeneic and xenograft models [5–8]. In addition, higher expression of BRMS1 in breast, lung, and melanoma cancers is associated with improved patient survival [8–10]. Despite promising functional evidence and clinical correlations, the mechanism by which BRMS1 blocks metastasis is yet to be understood.

BRMS1 is a known member of Sin3 histone deacetylase (HDAC) transcriptional regulatory complexes in multiple eukaryotic cell types [11–13]. It is a well-established binding partner of SUDS3 and ARID4A and is also associated with several other members of the epigenetics-modifying complex containing SIN3A, SIN3B, HDAC1, and HDAC2 [11]. However, BRMS1's exact function within the complex has yet to be defined. Intriguingly, the complex's scaffolding proteins, SIN3A and SIN3B, lack functional redundancy, a matter of significance as SIN3A has been shown to suppress metastasis, while SIN3B has been shown to promote it [14]. Molecularly, SIN3A is known to maintain a cell's pluripotent state, while SIN3B does not have the same effect [15]. Knockouts of either result in early embryonic or late embryonic lethality (SIN3A and SIN3B, respectively) indicating differences in early developmental roles [16, 17]. Understanding BRMS1's relationship to the two complexes, whether it be with SIN3A or SIN3B, could determine how BRMS1 functions to suppress metastasis. Relatedly, BRMS1 also exhibits E3 ubiquitin ligase function on the histone acetyl transferase p300, which could also be involved in its regulation of metastatic function [18]. Collectively, it appears that BRMS1 regulation of transcription via epigenetic pathways may be involved in suppression; however, further studies must be completed to ascribe a definitive mechanism of action.

In order to translate BRMS1 into clinical practice, additional structural and interactome data are necessary. This study leverages previously described features of BRMS1 to clarify its molecular functions within a cell. Previous attempts to define BRMS1 structure-function have been met with uneven success. To date no one has successfully crystallized nor determined structure for full-length, wild-type BRMS1. Computer algorithms and NMR studies have identified structural information for BRMS1 domains [19]. BRMS1 has predicted protein domains that consist of glutamate-rich regions (aa 1–50), two coiled-coil domains (aa 51–81, aa 147–180), and a nuclear localization sequence (aa 198–205) [5]. The N-terminus has been characterized and its 3D structure crystalized [20, 21], but outside of amino acids 51–98 there is no precise protein structure for the entirety of the 246 amino acid BRMS1 protein.

The C-terminus of the BRMS1 protein is of particular interest as it has been shown to play a critical role in metastatic suppression, due to *in vivo* studies demonstrating that alteration of the domain impacts overall metastatic burden [22]. Of note, the serine immediately upstream of the critical metastasis suppressor domain was found to be phosphorylated by Cyclin Dependent Kinase 2 (CDK2) [23]. Due to the juxtaposition of S237 to the C-terminal metastasis suppression region, this study focused on identifying proteins with which BRMS1 interacts within that domain as well as testing how phosphorylation within that domain can alter how BRMS1 regulates metastasis suppression, the results of which can be used to better understand how BRMS1 may function to suppress metastasis.

Materials and methods

Cloning of N-terminally halo-tagged versions of BRMS1 in pcDNA5/FRT

The BRMS1 primers listed in S1 Data were used to amplify a sequence coding for BRMS1 isoform 1 (NP_056214), or for mutant versions of BRMS1 as indicated in the figure legends,

using a previously reported BRMS1 construct as a template [24]. A short synthetic duplex DNA oligonucleotide (described in S1 Data) was used to clone a short fragment of the C terminus of BRMS1 (amino acids 230–246). DNA fragments were digested with SgfI and PmeI and inserted between SgfI and PmeI sites in pcDNA5FRT-Halo [12].

Affinity purification of BRMS1 for proteomic analysis

HEK293T cells (1×10^7) were cultured into a 15 cm tissue culture plates for 24 hours then Halo-BRMS1 constructs were transfected using Lipofectamine LTX (Thermo Fisher Scientific). After 48 hours cells were harvested and washed twice with ice-cold PBS. Cells were then resuspended in mammalian cell lysis buffer (Promega) (50 mM Tris·HCl (pH 7.5), 150 mM NaCl, 1% Triton® X-100, 0.1% sodium deoxycholate, 0.1 mM benzamidine HCl, 55 μM phenanthroline, 1 mM PMSF, 10 μM bestatin, 5 μM pepstatin A, and 20 μM leupeptin) followed by centrifugation at 21,000 × g for 10 min at 4˚C. To remove insoluble materials, cell extracts were diluted with 700 μl of TBS (50 mM Tris·HCl pH 7.4, 137 mM NaCl, 2.7 mM KCl) and centrifuged at 21,000 × *g* for 10 min at 4˚C. Next, cell extracts were incubated overnight at 4˚C with magnetic beads (Magne™ HaloTag® slurry). Before elution, magnetic beads were washed four times with wash buffer (50 mM Tris-HCl pH 7.4, 137 mM NaCl, 2.7 mM KCl, and 0.05% Nonidet® P40). Proteins bound to magnetic beads were eluted for 2 hours at room temperature using elution buffer containing 50 mM Tris-HCl pH 8.0, 0.5 mM EDTA, 0.005 mM DTT, and 2 Units AcTEV™ Protease (Thermo Fisher Scientific). The eluate was further purified by passing through a Micro Bio-Spin column (Bio-Rad, Hercules, CA) to remove residual beads prior to proteomic analyses.

MudPIT analysis for BRMS1 and BRMS1 mutant associated proteins

MudPIT analysis for protein identification was previously reported in detail by Banks *et al*. [12]. Briefly, trichloroacetic acid (TCA) precipitated proteins were proteolytically digested with endoproteinase Lys-C and trypsin digestion, respectively. Digested peptides were injected directly into a linear ion trap (LTQ) mass spectrometer using 10-step MudPIT separation approach, then the yielded spectra were collected and identified. Spectra were analyzed using the ProLuCID and DTASelect algorithms. Contrast and NSAF7 software were used, respectively, to rank putative affinity purified proteins according to their distributed normalized spectral abundance values (dNSAF). QSPEC was used to identify enriched proteins in the experimental samples [12].

Cross-linking analysis

Cross-linking data were utilized from publicly available data published by Adams et. al 2020 [25]. The BRMS1 cross-links were visualized within the xiView platform [26].

Topological scoring

Topological Scoring was completed for all proteins as previously described [27, 28]. Briefly, proteins with significant QSPEC scores were input into the TopS Shiny Application (available at https://github.com/WashburnLab/Topological-score-TopS). This application utilizes the average spectral counts of each bait across all baits to calculate the TopS score, which indicates a likelihood ratio of binding.

Protein structure predictions

BRMS1 protein structure was predicted based upon its amino acid sequence retrieved from NCBI using I-TASSER [29, 30]. Briefly, this program functions predicts, with high accuracy, protein structure based upon primary amino acid sequences by comparing the inputted sequence to known BLAST sequences. This comparison is then used to identify potential protein relatives, followed by threading, in which the LOMETS database utilizes the PDB database to generate alignments. Alignments with sufficient Z-Scores are then excised and assembled. Predicted structures are then subjected to iterative Monte Carlo simulations within a variety of conditions (temperature change simulations, etc.). Predictions with the lowest energy state are selected to be the predictive protein structures before comparing against knowns in the PDB database for structure, ligand binding, and biological function.

Protein stability predictions

The primary sequence of BRMS1 was mutated at S237 to either Aspartic Acid (D) or Alanine (A). These mutants were subject to multiple predictive software applications. MuPro [31] utilizes multiple machine learning techniques to predict the impact a point mutation has on protein stability. I-Mutant [32] is a support vector machine-based tool that functions by utilizing neural networks to predict protein stability changes based upon point mutations. Folding RaCe [33] predictive software utilizes a 790 single point mutant knowledge-based prediction of protein folding rates with a multiple linear regression model approach to predict the impact of single site mutations on folding rates. DynaMut [34] combines normal mode analysis which approximates system dynamics and motions with the mutational analysis, such that the prediction is based upon the impact that the mutation has on overall protein dynamics. DIM-Pred [35] predicts order or disorder of a protein or a protein region, accounting for alterations in amino acid properties, neighboring amino acids residues, and substation matrices.

Data analysis

Three biological replicates were performed for each bait protein (i.e., BRMS1 wild-type and four mutants). The distributed normalized spectral abundance factor (dNSAF) [36] was used to quantify the prey proteins in each bait AP-MS. To eliminate potential nonspecific proteins, three negative controls were analyzed from cells expressing the Halo tag alone. A total of 15 purifications were completed and 5085 prey proteins identified (S1 File). First, wild-type data were compared against the negative control dataset to ensure that non-specific proteins were not included in the analysis (S1 Table). Second, QSPEC [37] was used on this filtered protein list to calculate Z-statistics between spectral counts measured in wild-type and mutants and determine significant changes in protein levels between these two datasets (S2 Table). We retained only proteins that had a significant QSPEC Z-statistics of −2 or less in at least one of the mutants. The final group of 1175 proteins that passed these criteria comprised the subunits of the Sin3/HDAC complex and proteins outside the complex.

t-SNE

To spatially map all significant 1175 proteins, we first applied a T-Distributed Stochastic Neighbor Embedding (t-SNE), a nonlinear visualization of the data followed by a k-means clustering on the two vectors generated from the t-SNE (S2 Table). The number of clusters used for the k-means was 4. The plot visualization was generated within the R packages stats, cluster, gplots, and ggplot2.

Co-immunoprecipitation and MALDI-TOF analysis

To compare the overall composition of SIN3A associated proteins between metastatic and normal breast cells, co-IP of SIN3A (polyclonal Ab generated and validated previously [14]) from the nuclear lysates of MDA-MB-231 metastatic breast cancer and MCF10A immortalized but otherwise normal breast epithelial cell lines were analyzed by mass spectrometry. The co-IP samples were electrophoresed followed by in-gel digestion and MALDI-TOF analysis as previously described [38].

Pathway analysis

In order to determine the biological enrichment of differentially expressed proteins in the mutants, we subjected 1175 proteins to Reactome pathway analysis. Enrichment was completed within the R environment and several packages such as clusterProfiler, ReactomePA, DOSE and enrichplot were used.

Protein functional analysis

Significant proteins were subjected to multiple analyses. Disease enrichment was completed within Ingenuity Pathway Analysis (IPA, http://www.ingenuity.com, Release date: December 2016). Visualization for overlapping significant proteins was completed in Venny 2.1 (https://bioinfogp.cnb.csic.es/tools/venny/). Heatmaps were generated within ClustVis (https://biit.cs.ut.ee/clustvis/).

Cell culture

293T cells were cultured in 10% FBS, 0.5 mM NEAA + DMEM/Sodium Bicarbonate (2.438 g/L) cell culture medium (Thermo Fisher Scientific). MDA-MB-231 cells were cultured in 5% FBS, 0.5 mM NEAA 0 + DMEM/Sodium Bicarbonate (2.438 g/L) cell culture medium (Thermo Fisher Scientific). In both 293T and MDA-MB-231s, overexpression cells were first transduced with pENTR followed by pLENTI expression within 293FT cells according to manufacturer's instructions (Invitrogen). Clones were selected with blasticidin. Each construct contained a single or 3x-Flag epitope tag. Expression was quantified using validated BRMS1 1a5.7 antibody (as described previously [39]), FLAG-M2 antibody (Sigma A8592-IMG), or qPCR for $BRMS1^{230\text{-}246}$ using the following primers:

F: 5′- GATCCATGGACTACAAAGACCATGACGGTGATTATAAAGATCATGACATCGATTACA
AGGATGACGATGACAAGAAGGCTAGGGCAGCTGTGTCCCCTCAGAAGAGAAAATCGGAT
GGACCTTGATGATGAC -3′, R: 5′ -TCGAGTCATCATCAAGGTCCATCCGATTT
TCTCTTCTGAGGGGACACAGCTGCCCTAGCCTTCTGTCATCGTCATCCTTGTAATCGA
TGTCATGATCTTTATAATCACCGTCATGGTCTTTGTAGTCCATG -3′.

Predicted amino acid sequences for each construct are:
$BRMS1^{WT}$

DYKDDDDKMPVQPPSKDTEEMEAEGDSAAEMNGEEEESEEERSGSQTESEEES-
SEMDDEDYERRRSECVSEMLDLEKQFSELKEKLFRERLSQLRLRLEEVGAERAPEY-
TEPLGGLQRSLKIRIQVAGIYKGFCLDVIRNKYECELQGAKQHLESEKLLLYDTLQ-
GELQERIQRLEEDRQSLDLSSEWWDDKLHARGSSRSWDSLPPSKRKKAPLVSGPYI-
VYMLQEIDILEDWTAIKKARAAVSPQKRKSDGP

$BRMS1^{1\text{-}229}$

DYKDDDDKMPVQPPSKDTEEMEAEGDSAAEMNGEEEESEEERSGSQTESEEES-
SEMDDEDYERRRSECVSEMLDLEKQFSELKEKLFRERLSQLRLRLEEVGAERAPEY-
TEPLGGLQRSLKIRIQVAGIYKGFCLDVIRNKYECELQGAKQHLESEKLLLYDTLQ-
GELQERIQRLEEDRQSLDLSSEWWDDKLHARGSSRSWDSLPPSKRKKAPLVSGPYI-
VYMLQEIDILEDWTAI

S237A

DYKDDDDKMPVQPPSKDTEEMEAEGDSAAEMNGEEEESEEERSGSQTESEEES-
SEMDDEDYERRRSECVSEMLDLEKQFSELKEKLFRERLSQLRLRLEEVGAERAPEY-
TEPLGGLQRSLKIRIQVAGIYKGFCLDVIRNKYECELQGAKQHLESEKLLLYDTLQ-
GELQERIQRLEEDRQSLDLSSEWWDDKLHARGSSRSWDSLPPSKRKKAPLVSGPYI-
VYMLQEIDILEDWTAIKKARAAVAPQKRKSDGP

S237D

DYKDDDDKMPVQPPSKDTEEMEAEGDSAAEMNGEEEESEEERSGSQTESEEES-
SEMDDEDYERRRSECVSEMLDLEKQFSELKEKLFRERLSQLRLRLEEVGAERAPEY-
TEPLGGLQRSLKIRIQVAGIYKGFCLDVIRNKYECELQGAKQHLESEKLLLYDTLQ-
GELQERIQRLEEDRQSLDLSSEWWDDKLHARGSSRSWDSLPPSKRKKAPLVSGPYI-
VYMLQEIDILEDWTAIKKARAAVDPQKRKSDGP

$BRMS1^{230\text{-}246}$

MDYKDHDGDYKDHDIDYKDDDDKKARAAVSPQKRKSDGP

Metastasis gene expression analyses with qRT-PCR

293T cells were grown to 90% confluency, collected and RNA extracted an RNA Isolation kit (Zymo Research). Following RNA extraction cDNA completed with the iScript cDNA synthesis kit (Bio Rad). qRT-PCR was completed with a SYBER Green assay, and cDNA loaded at a concentration of 50 ng/uL. The following primers were utilized for analysis:

Migration assay

Cells were cultured at a seeding density of 750,000 cells/well in 5% FBS, 0.5 mM NEAA + DMEM/Sodium Bicarbonate (2.438 g/L) media in 6-well plates (Thermo Fisher). After 48 hours cells were scratched, washed, and media replaced with serum-free DMEM/Sodium Bicarbonate (2.438 g/L) (Thermo Fisher). Cells were imaged at t = 18 to 24 hrs. Image J (https://imagej.nih.gov/ij/) was utilized for analysis, followed by statistical analysis in R ('FAS' package), in which a Kruskal Wallis test followed by a Dunn's adjustment was completed (https://www.R-project.org/).

Experimental metastasis assays

To measure the successful colonization of the lungs by metastases for each construct ($BRMS1^{WT}$, S237A, or S237D) MDA-MB-231 cells were transduced with the construct as described above. For each construct, 3 clones were selected. $2x10^5$ cells suspended in 100 uL of Hanks Balanced Salt Solution (HBSS, Gibco, #14175–103) were intravenously injected within the tail vein of three week-aged athymic mice (Harlan HSD athymic nude-Foxn1nu), which

were restrained in a tube to facilitate tail manipulation. The lung metastases grew for 6 weeks or until the mouse was moribund and required euthanasia. Lungs were removed and fixed in a mixture of Bouin's fixative and neutral buffered formalin (1:5 v/v), and macroscopic lung metastases were counted. This study was completed in 30 mice per construct, and 3 clones per construct. All animal studies were approved by the Institutional Animal Care and Use Committee at the University of Kansas Medical Center (#2014–2208). These experiments were performed in accordance with the PHS Policy on Humane Care and Use of Laboratory Animals, USDA regulations (9 CFR Parts 1, 2, 3), the Federal Animal Welfare Act (7 USC 2131 et. Seq.), and the Guide for the Care and Use of Laboratory Animals, that were followed in attempts to alleviate animal suffering. A Kruskal Wallis test followed by a Dunn's adjustment was completed as per above for statistical analysis.

Clinical analyses

The UALCAN web resource was utilized to assess the expression of BRMS1, BRMS1L, HDAC1, SIN3A, and SUDS3 in tumor compared to normal expression (http://ualcan.path.uab.edu/index.html) [40]. All samples were within UALCAN's BRCA: Breast Invasive Carcinoma dataset. The normal dataset consisted of 114 patients, while the tumor contains 1097. Survival data were obtained from the 2020 version of Kaplan-Meier Plotter breast cancer RNA-sequencing database (https://kmplot.com/analysis/) [41]. Patients were first stratified by the Sin3/HDAC member (i.e., BRMS1L, HDAC1, SIN3A, SUDS3, 0etc.) by median. Once stratified BRMS1 expression was taken into account, and the p-value is calculated using the log-rank test.

Visualizations

R packages Gplots, GGplots2, and RColor Brewer were utilized for image analysis of data.

Results and discussion

BRMS1 C-terminal protein structure is important for protein-protein interactions, including Sin3/HDAC complex interaction

Utilizing our knowledge about BRMS1 from previously published functional and interaction studies we generated a panel of BRMS1 mutants: $BRMS1^{S237D}$ (phosphorylation-mimic, hereafter S237D); $BRMS1^{S237A}$ (unable to be phosphorylated, hereafter S237A); $BRMS1^{1\text{-}229}$ (lacks critical C-terminal domain); and $BRMS1^{230\text{-}246}$ (C-terminal domain with S237 in the center) (Fig 1A). Regardless of whether S237 was mutated to aspartic acid or alanine, BRMS1 protein stability was predicted to be compromised using multiple *in silico* prediction methods (Table 1). These data suggest that S237 site modifications dramatically destabilize BRMS1 and may be important for overall protein function and should be further investigated.

Given the lack of crystal structure for BRMS1 (and specifically the C-terminus), we used the I-Tasser structure prediction method to predict the three-dimensional structure of BRMS1 using its amino acid sequence (Fig 1B and 1C). The algorithm-predicted structure identifies that the C-terminal region may consist of helical, coiled, and strand regions, and the phosphorylation site of interest lies within a coiled domain (Fig 1B). The predicted coiled domain, coupled with a previous classification of this region as intrinsically disordered—both of which are associated with protein-protein interactions—supported our hypothesis that the region is involved with protein binding and that the interactome is involved in metastasis suppression [19].

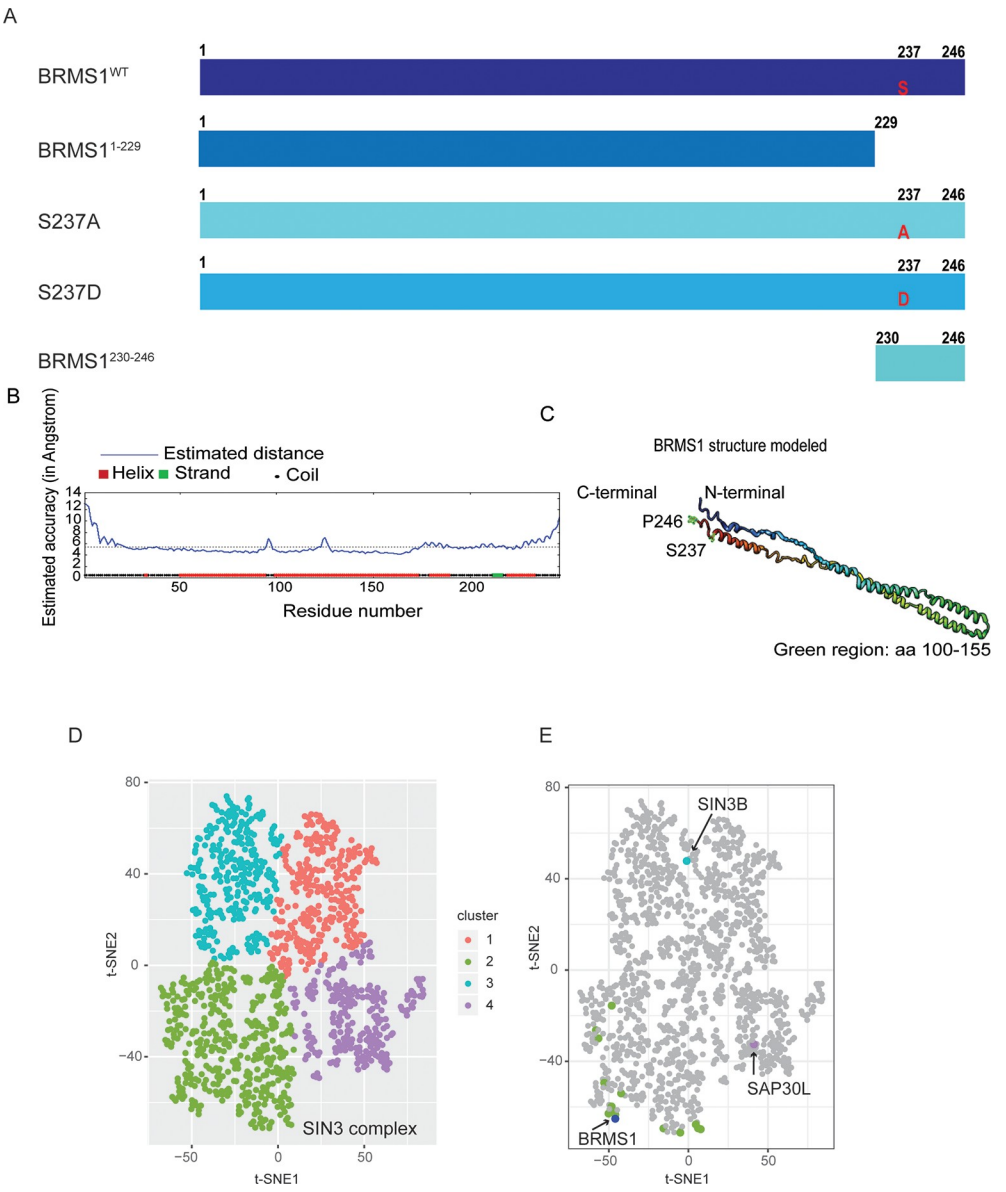

Fig 1. BRMS1 C-terminus plays a role in its protein interactome. (A) Mass spectrometry was completed on four BRMS1 mutants with full-length BRMS1 ($BRMS1^{WT}$), BRMS1 aa 1–229 ($BRMS1^{1-229}$), BRMS1 (S237A), BRMS1 (S237D), and BRMS1 aa 230–246 ($BRMS1^{230-246}$). (B). Secondary structure prediction of the BRMS1 proteins by I-TASSER, followed by the BRMS1 predicted 3D model (C). The structure generated demonstrates that the C-terminal region consists of helical, coiled, and strand regions. (D) t-SNE analysis was implemented for the analysis of the mutant data. Four clusters are generated by t-SNE. (E) Components of the Sin3/HDAC (in respective cluster colors from Fig 1D) and BRMS1 (in blue) proteins are highlighted.

https://doi.org/10.1371/journal.pone.0259128.g001

The I-TASSER and *in silico* prediction methods, when combined with our previous findings that S237 near the C-terminus can be phosphorylated compelled us to posit that the phosphorylation site could regulate protein binding. To test this hypothesis, mass spectrometry was completed (S1 Table) in 293T cells transduced with Halo-tagged BRMS1 wild-type ($BRMS1^{WT}$), $BRMS1^{1-229}$, S237A, S237D, or $BRMS1^{230-246}$ (Fig 1A). Constructs were precipitated via Halo-tags to prevent contamination with endogenous BRMS1. These constructs were selected because they allowed focus on both phosphorylation as well as putative protein

Target Gene	Primer
Cytochrome C	F- TTTGATGCCTTGGGTAGGG
	R- GACAAGCAGTGAGGGCTATT
Fascin	F- CTCTGGGTGTCTTGGTCTTT
	R—GGGCTGCAGACTGAGTTATT
miR-10b	F- CCCTGTAGAACCGAATTTGTG
	R—TTTGCATCGACCATATATTCCC
PI4K2NA	F–GAGCCCTATGGGCATCTTAATC
	R—GATAGCCCTGGTTAAGGACAAG
RhoC	F- CGTCCCTACTGTCTTTGAGAAC
	R- GCAGTCGATCATAGTCTTCCTG

https://doi.org/10.1371/journal.pone.0259128.t001

interaction domain(s). This point is key as BRMS1 contains two coiled-coil domains which are within BRMS1$^{1\text{-}229}$ but which are lacking in BRMS1$^{230\text{-}246}$, allowing us to identify proteins binding specifically to each region.

Mass spectrometry identified 1175 proteins whose binding was significantly (QSPEC Z-Score £-2) altered in at least one mutant compared to BRMS1^{WT}. In order to analyze the significant interacting proteins in an unbiased manner, we used the dimension reduction method t-Stochastic Neighbor Embedding (tSNE), applied to Z-statistics obtained from the QSPEC analysis [37]. This analysis resulted in four distinct clusters (Fig 1D, S2 Table). Further inspection identified BRMS1 as a member of cluster two, which contains the majority of the Sin3/HDAC members (Fig 1E). This finding reinforces BRMS1 membership within Sin3/HDAC complexes while also refining the interactome by lack of association of BRMS1 with SIN3B or SAP30L, which clustered differently (clusters 1 and 4, respectively) (Fig 1E).

BRMS1 interaction with Sin3/HDAC members is more complex than previously anticipated

To further examine the relationships between the Sin3/HDAC complex members and the BRMS1 mutants, Topological Scoring (TopS) was employed (Fig 2A). This method is used in

Table 1. Predicted protein stability is impacted by S237 mutations.

Mutant	Structure	Stability	Predicted Changes	Software
S237A	Primary	Destabilizing	DDG: -0.214633	MuProt
S237A	Primary	Destabilizing	DDG: -1.69	I-Mutant
S237A	Tertiary	Destabilizing	Folding Rate: -1.1	Folding Race
S237A	Primary	Destabilizing	DDG: -0.095	DynaMut
S237A	Tertiary	Destabilizing	DD Encom: -0.292 kcal/mol	DynaMut
S237A	Primary	Order → Disorder		DIM-Pred
S237D	Primary	Destabilizing	DDG: -0.0552	MuProt
S237D	Primary	Destabilizing	DDG: -1.0	I-Mutant
S237D	Tertiary	Destabilizing	Folding Rate: -1.8	Folding Race
S237D	Primary	Destabilizing	DDG: -0.457	DynaMut
S237D	Tertiary	Destabilizing	DD Encom: -0.353	DynaMut
S237D	Primary	Order → Disorder		DIM-Pred

Predictive software (listed) suggests that S237 plays a role in BRMS1 overall structure.

https://doi.org/10.1371/journal.pone.0259128.t002

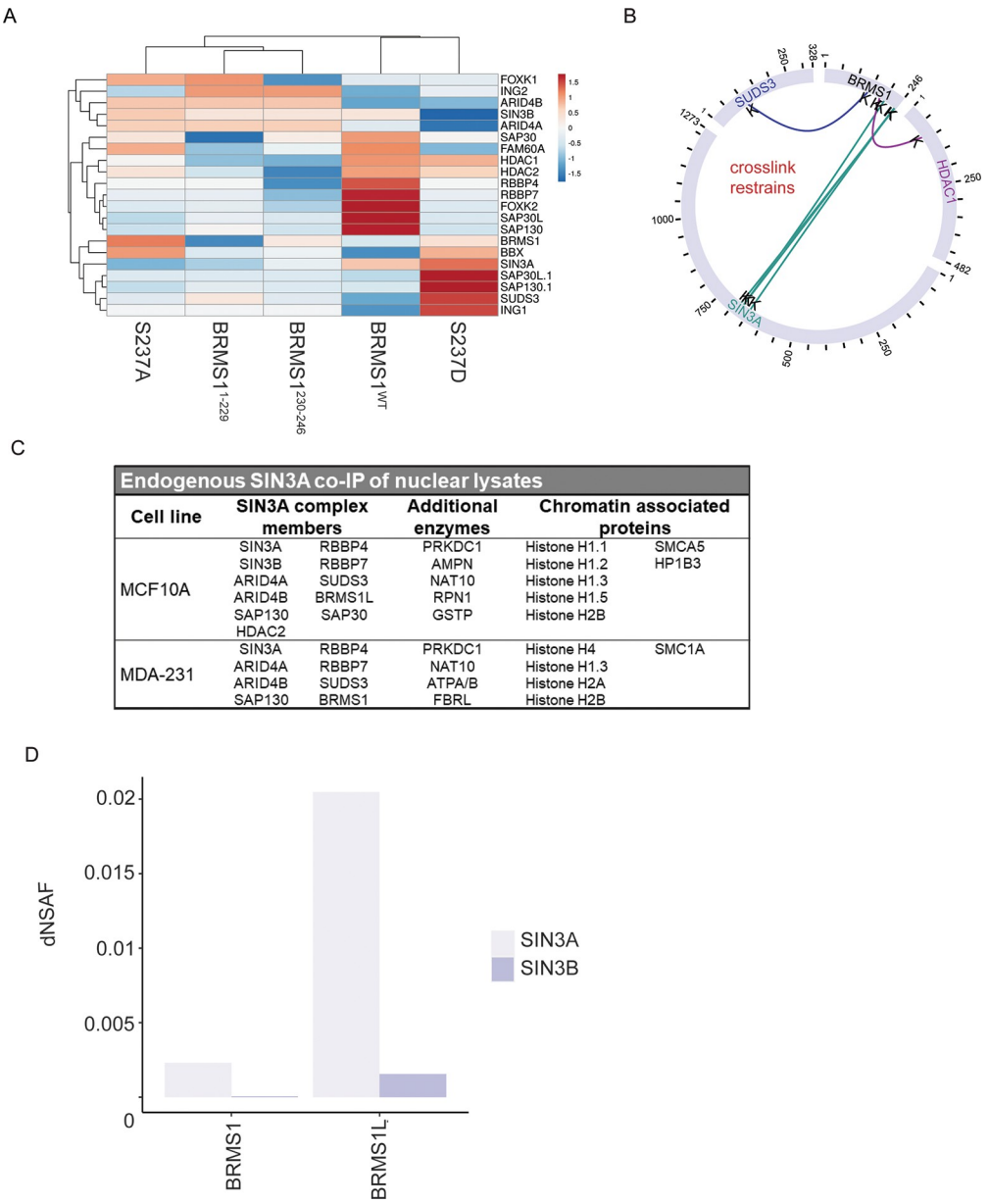

Fig 2. BRMS1 interacts with SIN3/HDAC members alternatively based protein domain. (A) Likelihood of binding for each SIN3A member was evaluation based on TopS score for each of the BRMS1 mutants. Cluster is based upon Euclidean distance. (B) Crosslink map for the BRMS1 protein, data is extracted from SIN3A XL-MS experiments from Adams et al [24]. (C) SIN3A co-immunoprecipitation of nuclear lysates followed by MALDI-TOF mass spectrometry. (D) Utilizing MS results from Adams et al [24] dNSAF for SIN3A and SIN3B in relation to BRMS1 and BRMS1L.

https://doi.org/10.1371/journal.pone.0259128.g002

determining a likelihood of binding with each of the proteins across the mutants. The resultant scoring suggests the presence or absence of S237 can play a role in BRMS1 interaction with protein complex members. Intriguingly, though there are some member interactions shared between S237A and S237D (BRMS1, BBX, and HDAC2), overall, the mutants' likely interaction partners tend to cluster differently (Fig 2A). S237A, BRMS1$^{1\text{-}229}$, and BRMS1$^{230\text{-}246}$ cluster the most similarly. This finding may suggest that in order for BRMS1^{WT} to interact with certain proteins it must include both phosphorylation at S237 as well as additional factors near

the N-terminus that BRMS1$^{230\text{-}246}$ lacks. That being said, BRMS1^{WT} and S237D have little overlap, sharing only HDAC1, HDAC2, and SIN3A (Fig 2A). This could be due to the fact that BRMS1^{WT} could more so exhibit a state of flux in regard to binding partners between its phosphorylated and unphosphorylated state and that it binds to many of these proteins, but this remains merely a hypothesis.

To further examine Sin3/HDAC complex binding with BRMS1 we utilized recently published crosslinking data of complex members [12]. BRMS1 was confirmed to interact with its known interaction partner SUDS3 (at BRMS1 aa 142), while also binding to the Sin3/HDAC member HDAC1 at BRMS1 aa 184 (Fig 2B). BRMS1 also cross-links with SIN3A but not with the related SIN3B (Fig 2B). Importantly, the location of SIN3A binding is primarily at BRMS1's C-terminus (at BRMS1 aa 201, 240, and 242) (Fig 2B). These data, in combination with the findings in Fig 1E, suggest that BRMS1 may impact the transcriptional profile of SIN3A complexes greater than SIN3B complexes. In addition, the location of the binding within the C-terminus supports the hypothesis that the C-terminus is involved in determining BRMS1's protein binding partners. Proximity of the binding sites (aa 240, 242) near S237 further supports the hypothesis that S237 phosphorylation plays a role in regulating BRMS1 binding partners. Taking the data into account with the findings in Fig 2A, the direct cross-link is associated with proteins more greatly associated with S237D (HDAC1, SIN3A, and SUDS3) than the other three mutants (Fig 2A) further suggesting the importance of phosphorylation and BRMS1's interaction within the Sin3/HDAC complex.

To examine the interaction between SIN3A and BRMS1 further, we utilized SIN3A-endogenously expressing cells. SIN3A was co-immunoprecipitated from the nuclear lysates of immortalized, but otherwise normal, MCF-10A breast cell line, as well as within the metastatic MDA-MB-231 breast cancer cell line. These precipitates were then subjected to mass spectrometry through MALDI-TOF analysis. Interactions with SIN3A were found to be context-dependent, i.e., normal breast cell line interactions differ from metastatic cancer cell interactions, though several of these interactions have been previously published and validated in many cell lines and systems (S3 Table, [11, 13, 22, 42–58]). SIN3A interacts with several Sin3/HDAC members in MCF-10A cells that it did not interact with in MDA-MB-231 (SIN3B, HDAC2, SAP30, BRMS1L). The only interactor that SIN3A interacted with in MDA-MB-231 that it lacked interaction with in MCF-10A is BRMS1. This finding is intriguing as BRMS1L and BRMS1 share high (79% amino acid) sequence similarity [59]. In terms of function, BRMS1L's role in metastasis is understudied, but two recent studies suggest a role in metastasis suppression [60, 61]. The finding that SIN3A binds to BRMS1 and BRMS1L differently in transformed and non-transformed cells (Fig 2C), suggests a role that BRMS1 plays within the Sin3/HDAC complex specifically in cancer that is not apparent in a non-transformed cell line.

To more clearly look at the interactions of BRMS1 and BRMS1L in association with the Sin3/HDAC complexes, we utilized normalized spectral counts of previously published mass spectrometry data [24]. We found a distinct pattern difference of BRMS1 and BRMS1L binding with SIN3A and SIN3B (Fig 2D). BRMS1L binds to a much greater extent to SIN3A than BRMS1. Though BRMS1L does not have spectral counts as great with SIN3B as it does to SIN3A, it must be noted that BRMS1 has a very low dNSAF score (5.64×10^{-5}) with SIN3B (Fig 2D). This finding, in combination with the findings in Figs 1E and 2B, compel the hypothesis that BRMS1 interacts with SIN3A over SIN3B. Additionally, the data suggest that BRMS1L may be more relevant in SIN3B complexes, and may also be more common in SIN3A directed complexes than BRMS1, as Fig 2C demonstrates. Taken in combination, these findings hint at a more specific role for BRMS1 within the Sin3/HDAC complex, and leaves room for potential functions independent of its interaction within these epigenetic regulatory complexes.

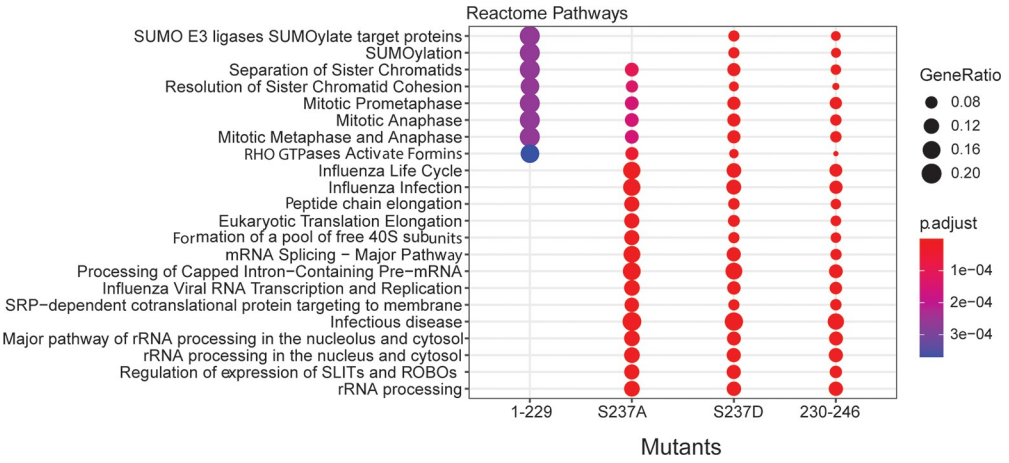

Fig 3. Biological pathway analysis associates BRMS1 mutants with specific molecular processes. The total number of 1175 proteins were subject to the Reactome pathway analysis. Top significant biological pathways with a p-value < 0.01 corresponding to the four mutants are represented in this figure.

https://doi.org/10.1371/journal.pone.0259128.g003

C-terminal mutants of BRMS1 disrupt protein interactions and molecular processes

Though significant that BRMS1 mutants altered binding with Sin3/HDAC members, many proteins that exist outside of those complexes also exhibited altered interactions with the mutants. To understand what biological processes may be disrupted due to altered protein interactions, all interacting proteins identified for each mutant were subjected to Reactome pathway analysis (Fig 3). Distinct differences in N-terminal (BRMS1$^{1\text{-}229}$) versus C-terminal (BRMS1$^{230\text{-}246}$) binding were observed. Many of the significant pathways represented in the analysis were not represented in BRMS1$^{1\text{-}229}$, e.g., mRNA processing, rRNA processing, and immune responses (Fig 3). Many of these same biological processes are disrupted by the C-terminus mutants (S237A, S237D, BRMS1$^{230\text{-}246}$), emphasizing the importance of the C-terminus in overall protein function and regulation of protein interactions. Importantly, many of the biological processes are tied to cancer-associated pathologies (i.e., mRNA splicing, immune response) and further study into the BRMS1 C-terminus role in these pathways could identify the molecular role of BRMS1 in metastasis. To identify binding partners distinctly affected by particular domains of BRMS1, all protein interaction changes for each mutant were considered. To ensure that putative interacting proteins were truly associated with BRMS1, an additional criterion was added, i.e., the interactor must have a high TopS value in BRMS1^{WT}, to demonstrate an increased likelihood of binding ratio (S4 Table) [27]. Significant overlaps between the C-terminus-associated mutants were observed. All three BRMS1 C-terminus mutants shared 64 proteins whose binding significantly changed compared to BRMS1^{WT} (Fig 4A and 4B). These results were in sharp contrast to BRMS1$^{1\text{-}229}$, in which those same 64 proteins shared a more similar binding profile to BRMS1^{WT} (Fig 4B). Several of the 64 proteins are known promiscuous binders [i.e., eukaryotic translation elongation factor 1 alpha 1 (EEF1A1), heterogeneous nuclear ribonucleoprotein F (HNRNPF)]. To filter promiscuous binders from unique interactors within this dataset, these 64 proteins were subjected to Contaminant Repository for Affinity Purification (CRAPome) analysis [27, 62]. Unique proteins were colored in red in Fig 4B. Several of these proteins are associated with cancer, such as TRMT2A (TRNA Methyltransferase 2 Homolog A) and WWP1 (WW Domain Containing E3 Ubiquitin Protein Ligase 1). TRMT2A is a methyltransferase protein and the expression of this

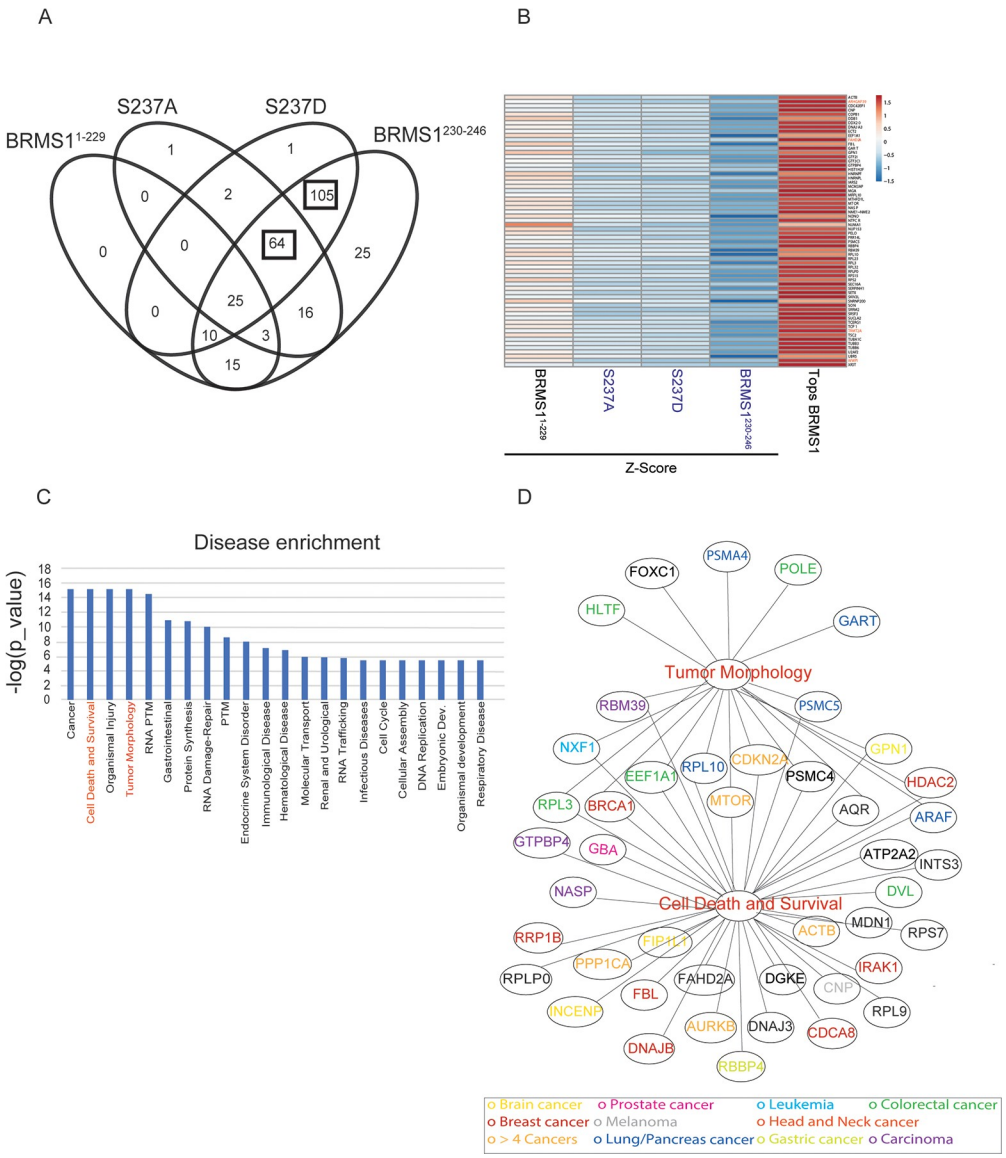

Fig 4. BRMS1 C-terminal binding partners are associated with known pathologies. (A) Venn diagram illustrating the shared proteins between the four mutants. Proteins shared between the three mutants located on the C-terminal and the shared subunits between the S237D and BRMS1$^{230-246}$ are indicated by a black box. (B) The z-statistics and the TopS values of the 64 proteins shared between the mutants located on the C-terminal are illustrated in (B). The red color corresponds to highest values (Tops or Z-statistics) whereas blue color indicates lower values. Proteins are colored in red if they are in the CRAPome database in less than 3/411 controls with maximum 1 Spectral count. (C) Disease enrichment. Proteins showing significant changes in the mutants in the C-terminal were used in the IPA analysis to determine the most enriched diseases within these proteins. Top 10 enriched classes are displayed in the Fig 4C. (D) Proteins in the tumor morphology class are illustrated in here. The proteins in the network were color coded according with the type of associated cancer.

https://doi.org/10.1371/journal.pone.0259128.g004

gene varies during the cell cycle, with aberrant expression being a possible biomarker in certain breast cancers [63]. Likewise, WWP1 is involved in breast mucinous carcinoma [64]. Two mutants, S237D and BRMS1$^{230-246}$, overlap with the most proteins, with 105 interactors (Fig 4A). These proteins were also subjected to CRAPome analysis, which identified several proteins as unique interactors. Two proteins were associated with metastasis, DNA Polymerase

Epsilon Subunit 2 (POLE2) and Transcription Factor 2 (TCF2) [65, 66]. POLE2 is associated with circulating tumor cell clusters which, in turn, have been associated with an increased colonization success [65]. TCF2 plays a role in renal cell carcinoma patient progression [67]. In combination, these findings further support the role the C-terminus plays in protein specific binding, while emphasizing the importance of phosphorylation-status on that interaction, and potentially disease state.

To further characterize how changes in interactor binding may play a role in the development of certain pathologies, disease enrichment within Ingenuity Pathway Analysis (IPA) was completed (Fig 4C and S5 Table (Worksheet 2)). This analysis included all interactor proteins with the C-terminus mutants (S237A, S237D, and BRMS1$^{230\text{-}246}$). Several of the enriched pathologies are often associated with neoplasia, including cell cycle dysregulation, cell death and survival, RNA damage repair, embryonic development, immunological disease, and infectious disease. The latter findings compliment previously published results in which re-expression of BRMS1 in metastatic MDA-MB-435 cells were highly enriched for upregulated immune response genes [68].

Two disease-associated categories were enriched and of distinct interest. The first, tumor morphology, is of interest as previous studies showed that BRMS1 re-expression alters expression of the cytoskeletal proteins Focal Adhesion Kinase (FAK), Src, and Fascin [69–71]. These proteins may ultimately change cell morphology and motility [72], which are essential for cancer metastasis [1] (Fig 4D). Additionally, enrichment for cell death and survival pathways mirror previous findings as BRMS1 is associated with inducing apoptosis in prostate and non-small cell lung cancers [73, 74]. BRMS1 is also associated with HDAC1 and NF-κB, both of which regulate apoptosis [74].

Within these two enriched disease pathways, several proteins overlap, including BReast CAncer gene 1 (BRCA1), mechanistic target of rapamycin (mTOR), and Cyclin Dependent Kinase Inhibitor 2A (CDKN2A) (Fig 4D). Several of the proteins, shared or not, have been associated with many cancers (Fig 4D). Proteins that are associated with the C-terminus of BRMS1 strongly suggests that the phosphorylation status of S237 plays roles not only in how BRMS1 functions within the cellular environment, but a distinct role that may shape the metastatic potential. This conclusion is consistent with previous reports that BRMS1 alters multiple steps in the metastatic cascade [69–71, 75].

BRMS1 domain and phosphorylation status may impact metastatic gene association

To test the impact of phosphorylation site presence or status on known metastasis-associated genes we measured expression changes on genes previously published to be regulated by BRMS1 [71, 76–79] (Fig 5A). To better translate findings from Figs 3 and 4 we completed qRT-PCR in 293T cells that were transduced with BRMS1^{WT} and its mutants (S1 Fig). As these measurements were performed in a non-cancerous cell line, many of the changes that have been reported in cancer cells were not expected to be identical. For example, phenotypes necessary for the cells' metastatic features would be expectedly low so that measurement of BRMS1 diminishment of expression from baseline would be insignificant. This is true for Fascin, PI4K2NA, and RhoC, all of which would be expected to be downregulated, but had no changes within 293T cells (Fig 5A). The only significant change was in miR-10b, which was downregulated as expected [79]. Interestingly, miR-10b was only significantly decreased in S237D and BRMS1$^{230\text{-}246}$ (Fig 5A), suggesting that BRMS1 regulation could be dependent on the presence of S237 and its phosphorylation. This result explains previous findings that BRMS1 C-terminus is responsible for regulating miR-10b expression and points to BRMS1

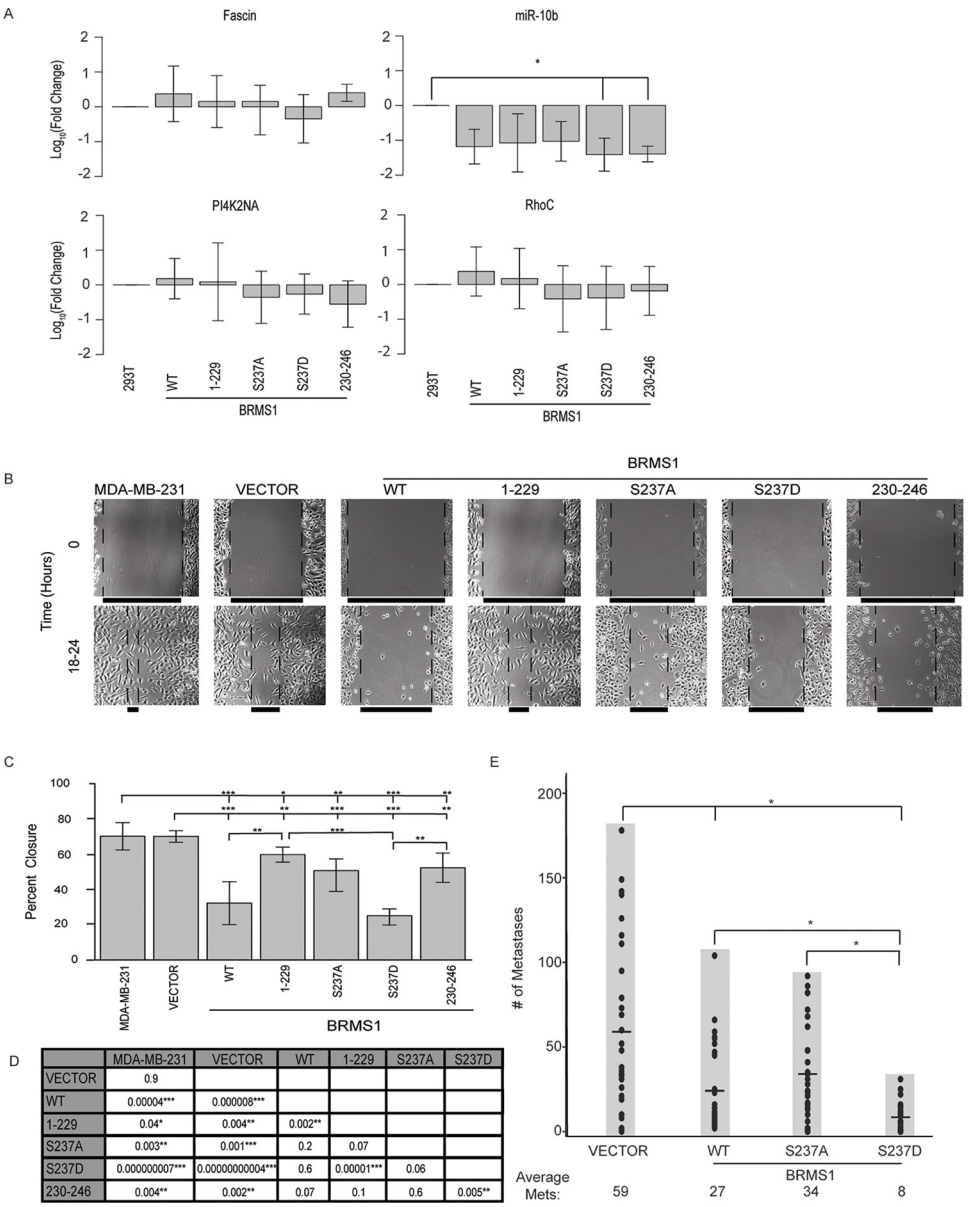

	MDA-MB-231	VECTOR	WT	1-229	S237A	S237D
VECTOR	0.9					
WT	0.00004***	0.000008***				
1-229	0.04*	0.004**	0.002**			
S237A	0.003**	0.001***	0.2	0.07		
S237D	0.000000007***	0.00000000004***	0.6	0.00001***	0.06	
230-246	0.004**	0.002**	0.07	0.1	0.6	0.005**

Fig 5. BRMS1 phosphorylation is associated with a metastasis suppression phenotype. (A) Average qRT-PCR results for 293T cells transduced with $BRMS1^{WT}$, $BRMS\ 1^{1-229}$, S237A, S237D, or $BRMS1^{230-246}$. Quantification includes 3 clones per construct and an n = 3. Samples were analyzed with a Kruskal Wallis test, followed by a Dunn's adjustment. * indicates p -values ≤ 0.05. (B) Representative images for migration analysis on parental MDA-MB-231, Vector (control) transduced MDA-MB-231s, $BRMS1^{WT}$, $BRMS1^{1-229}$, S237A, S237D, and $BRMS1^{230-246}$ MDA-MB-231 transduced cells. (C) Quantification of migration assays, analyzed with a Kruskal Wallis test, followed by a Dunn's adjustment. *, **, and *** indicate p-values of ≤ 0.05, ≤ 0.01, and ≤ 0.001, respectively. (D) This table includes the p-values for the comparisons completed in (C). (E) IV Injections of MDA-MB-231 cells expressing vector, $BRMS1^{WT}$, S237A, or S237D. Each experimental group represents an n = 30. * indicates a p-value ≤ 0.05. Samples were analyzed with a Kruskal Wallis test, followed by a Dunn's adjustment.

https://doi.org/10.1371/journal.pone.0259128.g005

phosphorylation as a key factor that does so [22]. Further studies must be done to understand the importance of BRMS1 regulation of miR-10b, but the finding does suggest a potential role for S237's regulation of metastasis.

Domain and phosphorylation status alter MDA-MB-231 migration *in vitro* and lung metastases *in vivo*

To begin assessing whether BRMS1 mutants exert different biological changes in cancer cells, BRMS1 mutants were transduced into metastatic MDA-MB-231 breast carcinoma cells (S1 Fig). Scratch assays were performed to determine the impact of BRMS1 mutants on *in vitro* cell migration. All BRMS1 mutants inhibited migration (Fig 5B–5D). Curiously, $BRMS1^{230\text{-}246}$ reduced migration slightly more than $BRMS1^{1\text{-}229}$, but this comparison was not statistically significant. $BRMS1^{WT}$ and S237D expressing cells were significantly less migratory than $BRMS1^{1\text{-}229}$, while only S237D was less migratory than $BRMS1^{230\text{-}246}$. These data suggest that the capacity to exist within a phosphorylated state could decrease the migratory capacity. This observation is speculative, as neither S237A nor S237D have a statistically significantly different migratory capacity to $BRMS1^{WT}$, but the wound closure patterns are in opposite directions. Based upon the *in vitro* data, and the lack of significant difference between S237A and S237D, the full impact of phosphorylation-status is unclear but is suggestive of a role it may play in metastasis.

Based upon the migration data, and the definite differences implicating phosphorylation-status, we wanted to determine if BRMS1 phosphorylation was key to BRMS1-regulated metastasis suppression. To test this, we completed intravenous tail-vein injections with MDA-MB-231 cells expressing $BRMS1^{WT}$, S237A, or S237D (Fig 5E). Both $BRMS1^{WT}$ and S237D were significantly different to vector control, while S237A was not. In addition, S237D had a significant decrease in the number of lung metastases than either $BRMS1^{WT}$ or S237A. These findings suggest firstly the inability of BRMS1 to phosphorylate at S237 does impact metastasis suppressor function. Secondly, the degree of significance by which S237D is able to suppress metastasis, with a decrease compared to $BRMS1^{WT}$ and S237A strongly suggests the key role that S237 phosphorylation plays in BRMS1 metastasis suppression.

BRMS1 and SIN3 members may impact patient survival

As metastasis is associated with decreased overall patient survival, we questioned if the interactions within the Sin3/HDAC complex could play a role in impacting patient survival. Utilizing data from The Cancer Genome Atlas (TCGA), we examined how BRMS1 interacting partners (Fig 2B) as well as its counterpart, BRMS1L (Fig 2C), expression correlated in breast cancer patient survival.

Firstly, we compared the expression of the Sin3/HDAC members from normal to breast tumor samples. BRMS1, HDAC1 and SUDS3 significantly increase expression within the tumor samples, while BRMS1L has significantly decreased expression (Fig 6A). SIN3A is unchanged. This finding is intriguing as BRMS1 directly binds both HDAC1 and SUDS3, and hints at a potential association with their expression and patient survival.

To address this speculation, we also looked for an association between one of the Sin3/HDAC members and BRMS1 expression. To do this we first separated patients by expression of each Sin3/HDAC BRMS1-interacting member by expression greater than or less than the median expression of that particular member. Within those subsets, BRMS1 expression (high vs low) was examined for patient overall survival (Fig 6B and 6C). When looking across all Sin3/HDAC members associated with a high median expression cohort, BRMS1 does not appear to play a role in increased patient survival (Fig 6B). In fact, we only see an association with patient survival in the low expression cohorts of BRMS1L and SIN3A, in which high expression of BRMS1 is associated with increased patient survival (p-value of 0.019 and 0.021, respectively) (Fig 6C). Interestingly, this pattern is similar in the rest of the Sin3/HDAC complex members, in which across all members in the high-expressing cohort, BRMS1 expression did not play a role (S2 Fig). However, in the low-expressing cohort, BRMS1 high expression

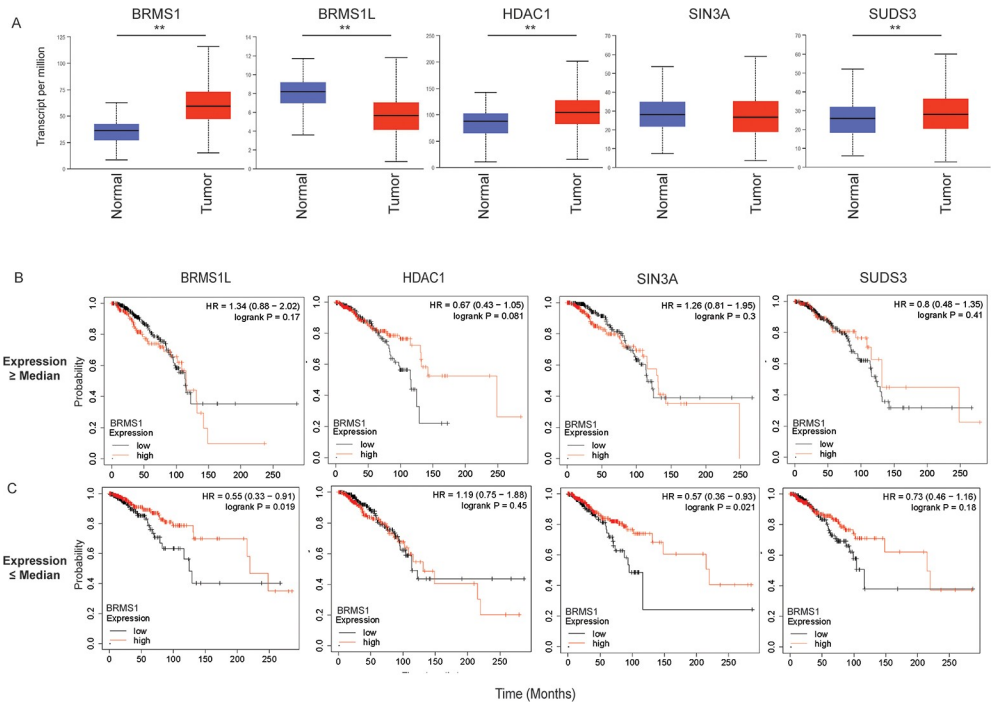

Fig 6. SIN3/HDAC members have altered impact on breast cancer outcomes. (A) Breast Cancer (BRCA) data from TCGA was mined utilizing UALCAN to determine differences in expression of normal compared to tumor tissue. ** indicates a p-value < 0.01. (B-C). BRCA data was mined in which SIN3/HDAC members were separated by median expression into those greater than the median (B) or those less than the median (C). BRMS1 expression was then examined within these patients for overall survival, with High BRMS1 (indicated by Red) and Low BRMS1 (indicated by black) were accounted for. This was completed in KM Plotter.

https://doi.org/10.1371/journal.pone.0259128.g006

plays a role in overall survival for BBX and SAP130 (S3 Fig). As previously noted, BRMS1L appears to play a role in metastasis suppression. It has also been shown that low expression of SIN3A promotes invasion and metastasis, and increased SIN3A expression is associated with increased overall survival [14]. Additionally, both SAP130 (Sin3A Associated Protein 130) and BBX have been directly associated with binding SIN3A [45, 80]. Decreased SAP130 expression has been associated with metastasis previously [81]. These previously published findings, in combination with our results, may suggest that in either low BBX, BRMS1L, SAP130, or SIN3A expressing patients BRMS1 expression will take on the role of a metastasis suppressor, resulting in increased overall survival. However, if BBX, BRMS1L, SAP130, or SIN3A expression is high, BRMS1 expression is not as critical in terms of overall survival as the breast cancer itself should not be highly invasive or metastatic (Figs 6B and S2). Though these data require further testing to be conclusive, they further our understanding of BRMS1's role in relation to the SIN3/HDAC complex, and how this interaction may be key to understanding how this is associated with metastasis.

Conclusions

This study investigates the role of BRMS1 C-terminus in protein function, with an emphasis on the function of the S237 phosphorylation site. We hypothesized, based upon *in silico* prediction methods, that the C-terminus functions in protein binding, and demonstrated through mass spectrometry that the C-terminus can impact BRMS1 associations with Sin3/HDAC complexes as well as proteins outside of the complexes. We model this hypothesis in Fig 7, in

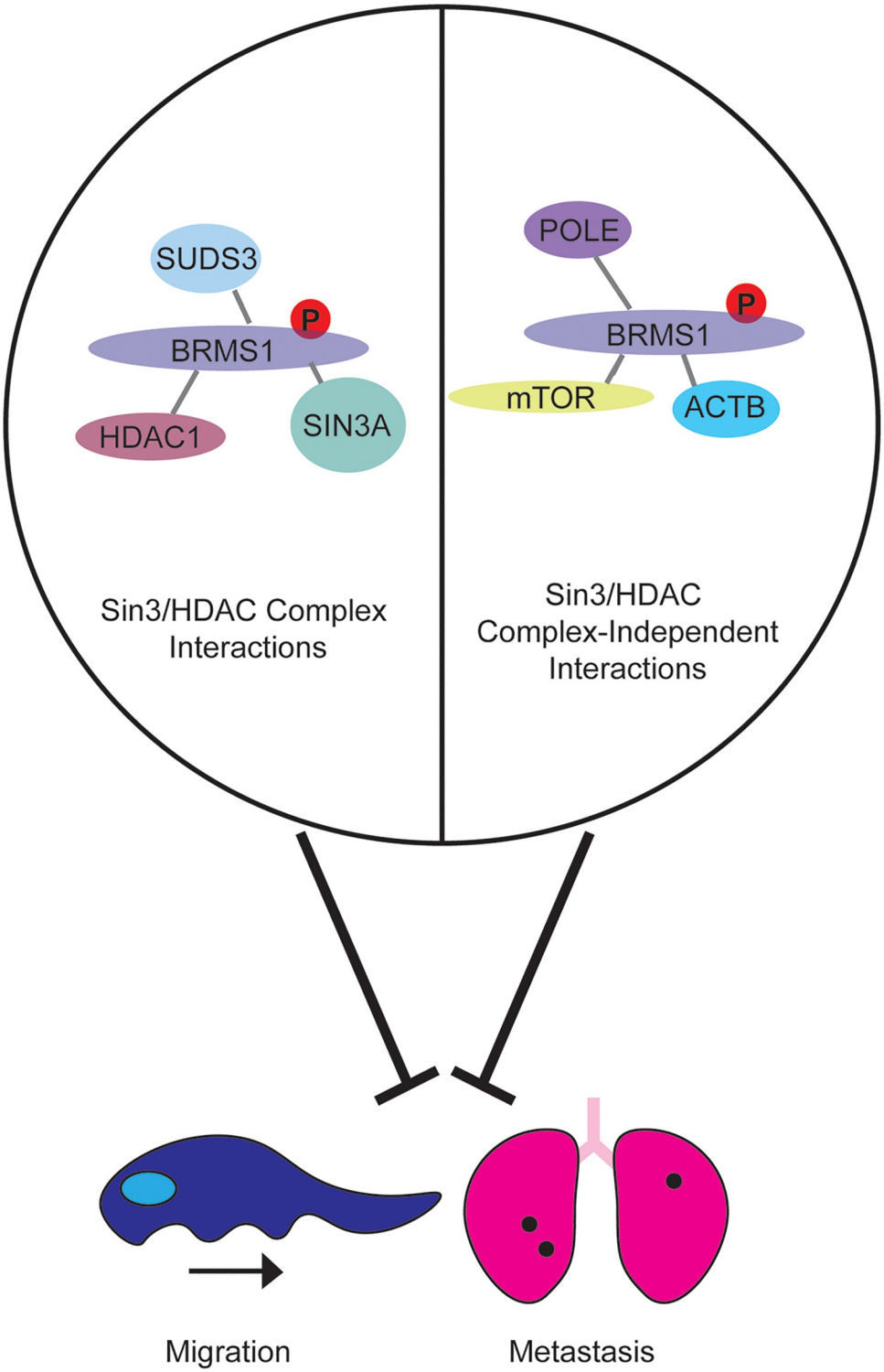

Fig 7. Phosphorylation at S237 contributes to the anti-metastatic phenotype of BRMS1 and alters BRMS1 protein interactions. BRMS1 associates with Sin3/HDAC complex members as well as other proteins which are not part of the chromatin remodeling complexes. We hypothesize that BRMS1 phenotypes are determined by the proteins with which it interacts but cannot yet ascribe a specific cause-effect relationship responsible for metastasis or migratory suppression.

https://doi.org/10.1371/journal.pone.0259128.g007

which we believe that BRMS1 does indeed regulate its anti-metastatic function through altered interactions with proteins within or outside of the complex. This study probed both hypotheses by furthering the understanding of BRMS1 association with Sin3/HDAC by defining direct interactions with SIN3A, HDAC1, and SUDS3. We further define BRMS1's relationship with SIN3A and determined that it may play a more significant role in SIN3A associated complexes compared to that of SIN3B. We also further defined its relationship with BRMS1L and noticed that, despite sequence similarity, BRMS1 and BRMS1L did not appear to have a mirror image relationship to SIN3A or SIN3B. Future studies, that further examine the spatial and temporal interactions could be extremely beneficial to associate how the BRMS1 interactions play a role in pathologies such as metastasis. These findings could follow up the findings in Fig 2C as well as previously published BRMS1 localization data [22]. We did begin to assess how these interactions could impact pathologies, through examining the relationship that members of the Sin3/HDAC complex have with BRMS1 that is associated with overall survival.

It is interesting to speculate that once expression of either BRMS1L or SIN3A is lost, it appears that BRMS1 will then function to suppress metastasis and increase survival. Our data begin to define these interactions, in particular with SIN3A, but further studies are required in order to directly define those relationships, including whether the interactions are based on phosphorylation-status to regulate metastasis. The C-terminus and phosphorylation status appear to be vital to regulating the metastasis promoting miRNA miR-10b and corresponding reductions in motility and metastasis. The data also identify specific functionalities of protein complexes previously associated with BRMS1 and metastasis.

This combination of results refine the molecular impact of BRMS1 on regulating metastasis and the potential development of therapeutics based upon BRMS1.

Supporting information

S1 Fig. Expression of BRMS1 mutants within 293T and MDA-MB-231 cells. Expression of BRMS1WT, BRMS11-229, and phospho-mutants compared to parental and vector control 293T cells. (B) qPCR quantification of BRMS1230-246 expression in 293T cells. (C) Expression of BRMS1WT and phospho-mutants compared to vector control MDA-MB-231 cells. (D). Expression of BRMS11-229 within MDA-MB-231 cells. (E) qPCR quantification of BRMS1230-246 expression in MDA-MB-231 cells.
(TIF)

S2 Fig. Survival analysis for BRMS1 expression for patients with high expressing Sin3/HDAC members impact on overall survival. BRCA data was mined in which SIN3/HDAC members were separated by median expression into those greater than the median BRMS1 expression was then examined within these patients for overall survival, with high BRMS1 (indicated by Red) and low BRMS1 (indicated by black) were accounted for. This was completed in KM Plotter.
(TIF)

S3 Fig. Survival analysis for BRMS1 expression for patients with low expressing Sin3/HDAC members impact on overall survival. BRCA data was mined in which SIN3/HDAC members were separated by median expression into those less than the median BRMS1 expression was then examined within these patients for overall survival, with high BRMS1 (indicated by Red) and low BRMS1 (indicated by black) were accounted for. This was completed in KM Plotter.
(TIF)

S1 Table. BRMS1 data statistics.
(XLSX)

S2 Table. t-SNE results on proteins that were significantly changing between BRMS1 wild-type and the mutants.
(XLSX)

S3 Table. SIN3A known interactors and validation method.
(DOCX)

S4 Table. Proteins that have high TopS scores in the BRMS1 wild-type and changing in the mutants.
(XLSX)

S5 Table. Reactome pathways analysis.
(XLSX)

S1 Raw images.
(TIF)

S1 File.
(XLSX)

S1 Data.
(DOCX)

Author Contributions

Conceptualization: Douglas R. Hurst, Michael P. Washburn, Danny R. Welch.

Data curation: Mihaela E. Sardiu, Christa A. Manton, Md. Sayem Miah, Charles A. S. Banks, Mark K. Adams, Mick D. Edmonds, Michael P. Washburn.

Formal analysis: Rosalyn C. Zimmermann, Mihaela E. Sardiu, Christa A. Manton, Md. Sayem Miah, Charles A. S. Banks, Mark K. Adams, Devin C. Koestler, Douglas R. Hurst, Mick D. Edmonds, Michael P. Washburn, Danny R. Welch.

Funding acquisition: Rosalyn C. Zimmermann, Devin C. Koestler, Michael P. Washburn, Danny R. Welch.

Investigation: Rosalyn C. Zimmermann, Mihaela E. Sardiu, Christa A. Manton, Md. Sayem Miah, Charles A. S. Banks, Mark K. Adams, Douglas R. Hurst, Mick D. Edmonds, Michael P. Washburn, Danny R. Welch.

Methodology: Christa A. Manton, Md. Sayem Miah, Charles A. S. Banks.

Project administration: Michael P. Washburn, Danny R. Welch.

Resources: Michael P. Washburn, Danny R. Welch.

Supervision: Devin C. Koestler, Michael P. Washburn, Danny R. Welch.

Validation: Rosalyn C. Zimmermann, Douglas R. Hurst.

Visualization: Danny R. Welch.

Writing – original draft: Rosalyn C. Zimmermann, Mihaela E. Sardiu, Christa A. Manton, Md. Sayem Miah, Charles A. S. Banks, Mark K. Adams, Michael P. Washburn, Danny R. Welch.

Writing – review & editing: Rosalyn C. Zimmermann, Mihaela E. Sardiu, Christa A. Manton, Md. Sayem Miah, Charles A. S. Banks, Mark K. Adams, Devin C. Koestler, Douglas R. Hurst, Mick D. Edmonds, Michael P. Washburn, Danny R. Welch.

References

1. Welch DR, Hurst DR. Defining the Hallmarks of Metastasis. Cancer Res. 2019; 79(12):3011–27. Epub 2019/05/06. https://doi.org/10.1158/0008-5472.CAN-19-0458 PMID: 31053634; PubMed Central PMCID: PMC6571042.
2. Liu Y, Mayo MW, Xiao A, Hall EH, Amin EB, Kadota K, et al. Loss of BRMS1 Promotes a Mesenchymal Phenotype through NF-kappaB-Dependent Regulation of Twist1. Mol Cell Biol. 2014. MCB.00869-14 [pii]; https://doi.org/10.1128/MCB.00869-14 PMID: 25368381
3. Steeg PS, Ouatas T, Halverson D, Palmieri D, Salerno M. Metastasis suppressor genes: Basic biology and potential clinical use. Clinical Breast Cancer. 2003; 5:51–62. https://doi.org/10.3816/cbc.2003.n.012 PMID: 12744759
4. Liu W, Vivian CJ, Brinker AE, Hampton KR, Lianidou E, Welch DR. Microenvironmental Influences on Metastasis Suppressor Expression and Function during a Metastatic Cell's Journey. Cancer Microenviron. 2014; 7(3):117–31. Epub 2014/06/19. https://doi.org/10.1007/s12307-014-0148-4 PMID: 24938990; PubMed Central PMCID: PMC4275500.
5. Seraj MJ, Samant RS, Verderame MF, Welch DR. Functional evidence for a novel human breast carcinoma metastasis suppressor, *BRMS1*, encoded at chromosome 11q13. Cancer Research. 2000; 60 (11):2764–9. WOS:000087434700005. PMID: 10850410
6. Seraj MJ, Harding MA, Gildea JJ, Welch DR, Theodorescu D. The relationship of *BRMS1* and *RhoGDI2* gene expression to metastatic potential in lineage related human bladder cancer cell lines. Clin Exp Metastasis. 2000; 18(6):519–25. Epub 2001/10/11. https://doi.org/10.1023/a:1011819621859 PMID: 11592309.
7. Shevde LA, Samant RS, Welch DR. Suppression of human melanoma metastasis by breast metastasis suppressor [BRMS1]. PNAS. 2001; 42:646.
8. Bucciarelli PR, Tan KS, Chudgar NP, Brandt W, Montecalvo J, Eguchi T, et al. BRMS1 Expression in Surgically Resected Lung Adenocarcinoma Predicts Future Metastases and Is Associated with a Poor Prognosis. J Thorac Oncol. 2018; 13(1):73–84. Epub 2017/11/04. https://doi.org/10.1016/j.jtho.2017.10.006 PMID: 29097253; PubMed Central PMCID: PMC5738269.
9. Li J, Cheng Y, Tai D, Martinka M, Welch DR, Li G. Prognostic significance of BRMS1 expression in human melanoma and its role in tumor angiogenesis. Oncogene. 2011; 30(8):896–906. Epub 2010/10/12. https://doi.org/10.1038/onc.2010.470 PMID: 20935672; PubMed Central PMCID: PMC3235331.
10. Zhang Z, Yamashita H, Toyama T, Yamamoto Y, Kawasoe T, Iwase H. Reduced expression of the breast cancer metastasis suppressor 1 mRNA is correlated with poor progress in breast cancer. Clin Cancer Res. 2006; 12(21):6410–4. Epub 2006/11/07. https://doi.org/10.1158/1078-0432.CCR-06-1347 PMID: 17085653.
11. Meehan WJ, Samant RS, Hopper JE, Carrozza MJ, Shevde LA, Workman JL, et al. Breast cancer metastasis suppressor 1 (BRMS1) forms complexes with retinoblastoma-binding protein 1 (RBP1) and the mSin3 histone deacetylase complex and represses transcription. J Biol Chem. 2004; 279(2):1562–9. Epub 2003/10/29. https://doi.org/10.1074/jbc.M307969200 PMID: 14581478.
12. Banks CAS, Zhang Y, Miah S, Hao Y, Adams MK, Wen Z, et al. Integrative Modeling of a Sin3/HDAC Complex Sub-structure. Cell Rep. 2020; 31(2):107516. Epub 2020/04/16. https://doi.org/10.1016/j.celrep.2020.03.080 PMID: 32294434; PubMed Central PMCID: PMC7217224.
13. Sardiu ME, Smith KT, Groppe BD, Gilmore JM, Saraf A, Egidy R, et al. Suberoylanilide hydroxamic acid (SAHA)-induced dynamics of a human histone deacetylase protein interaction network. Mol Cell Proteomics. 2014; 13(11):3114–25. Epub 2014/07/31. https://doi.org/10.1074/mcp.M113.037127 PMID: 25073741; PubMed Central PMCID: PMC4223495.
14. Lewis MJ, Liu J, Libby EF, Lee M, Crawford NP, Hurst DR. SIN3A and SIN3B differentially regulate breast cancer metastasis. Oncotarget. 2016; 7(48):78713–25. Epub 2016/10/27. https://doi.org/10.18632/oncotarget.12805 PMID: 27780928; PubMed Central PMCID: PMC5340233.
15. Saunders A, Huang X, Fidalgo M, Reimer MH Jr., Faiola F, Ding J, et al. The SIN3A/HDAC Corepressor Complex Functionally Cooperates with NANOG to Promote Pluripotency. Cell Rep. 2017; 18(7):1713–26. Epub 2017/02/16. https://doi.org/10.1016/j.celrep.2017.01.055 PMID: 28199843; PubMed Central PMCID: PMC5328122.
16. Cowley SM, Iritani BM, Mendrysa SM, Xu T, Cheng PF, Yada J, et al. The mSin3A chromatin-modifying complex is essential for embryogenesis and T-cell development. Mol Cell Biol. 2005; 25(16):6990–

7004. Epub 2005/08/02. https://doi.org/10.1128/MCB.25.16.6990-7004.2005 PMID: 16055712; PubMed Central PMCID: PMC1190252.

17. David G, Grandinetti KB, Finnerty PM, Simpson N, Chu GC, Depinho RA. Specific requirement of the chromatin modifier mSin3B in cell cycle exit and cellular differentiation. Proc Natl Acad Sci U S A. 2008; 105(11):4168–72. Epub 2008/03/12. https://doi.org/10.1073/pnas.0710285105 PMID: 18332431; PubMed Central PMCID: PMC2393767.

18. Liu Y, Mayo MW, Nagji AS, Hall EH, Shock LS, Xiao A, et al. BRMS1 suppresses lung cancer metastases through an E3 ligase function on histone acetyltransferase p300. Cancer Res. 2013; 73(4):1308–17. Epub 2012/12/28. https://doi.org/10.1158/0008-5472.CAN-12-2489 PMID: 23269275; PubMed Central PMCID: PMC3578176.

19. Pantoja-Uceda D, Neira JL, Contreras LM, Manton CA, Welch DR, Rizzuti B. The isolated C-terminal nuclear localization sequence of the breast cancer metastasis suppressor 1 is disordered. Arch Biochem Biophys. 2019; 664:95–101. Epub 2019/02/02. https://doi.org/10.1016/j.abb.2019.01.035 PMID: 30707944; PubMed Central PMCID: PMC6532052.

20. Spinola-Amilibia M, Rivera J, Ortiz-Lombardia M, Romero A, Neira JL, Bravo J. The structure of BRMS1 nuclear export signal and SNX6 interacting region reveals a hexamer formed by antiparallel coiled coils. J Mol Biol. 2011; 411(5):1114–27. Epub 2011/07/23. https://doi.org/10.1016/j.jmb.2011.07.006 PMID: 21777593.

21. Rivera J, Megias D, Bravo J. Sorting nexin 6 interacts with breast cancer metastasis suppressor-1 and promotes transcriptional repression. J Cell Biochem. 2010; 111(6):1464–72. Epub 2010/09/11. https://doi.org/10.1002/jcb.22874 PMID: 20830743.

22. Hurst DR, Xie Y, Thomas JW, Liu J, Edmonds MD, Stewart MD, et al. The C-terminal putative nuclear localization sequence of breast cancer metastasis suppressor 1, BRMS1, is necessary for metastasis suppression. PLoS One. 2013; 8(2):e55966. Epub 2013/02/08. https://doi.org/10.1371/journal.pone.0055966 PMID: 23390556; PubMed Central PMCID: PMC3563580.

23. Roesley SN, Suryadinata R, Morrish E, Tan AR, Issa SM, Oakhill JS, et al. Cyclin-dependent kinase-mediated phosphorylation of breast cancer metastasis suppressor 1 (BRMS1) affects cell migration. Cell Cycle. 2016; 15(1):137–51. Epub 2016/01/16. https://doi.org/10.1080/15384101.2015.1121328 PMID: 26771717; PubMed Central PMCID: PMC4825791.

24. Adams MK, Banks CAS, Thornton JL, Kempf CG, Zhang Y, Miah S, et al. Differential Complex Formation via Paralogs in the Human Sin3 Protein Interaction Network. Mol Cell Proteomics. 2020; 19(9):1468–84. Epub 2020/05/30. https://doi.org/10.1074/mcp.RA120.002078 PMID: 32467258; PubMed Central PMCID: PMC8143632.

25. Adams MK, Banks CAS, Thornton JL, Sardiu ME, Killer M, Kempf CG, et al. Differential complex formation via paralogs in the human Sin3 protein interaction network. bioRxiv. 2019:830828. https://doi.org/10.1101/830828

26. Graham M, Combe C, Kolbowski L, Rappsilber J. xiView: A common platform for the downstream analysis of Crosslinking Mass Spectrometry data. bioRxiv. 2019:561829. https://doi.org/10.1101/561829

27. Sardiu ME, Gilmore JM, Groppe BD, Dutta A, Florens L, Washburn MP. Topological scoring of protein interaction networks. Nat Commun. 2019; 10(1):1118. Epub 2019/03/10. https://doi.org/10.1038/s41467-019-09123-y PMID: 30850613; PubMed Central PMCID: PMC6408525.

28. Sardiu ME, Florens L, Washburn MP. Generating topological protein interaction scores and data visualization with TopS. Methods. 2020; 184:13–8. Epub 2019/09/03. https://doi.org/10.1016/j.ymeth.2019.08.010 PMID: 31476375; PubMed Central PMCID: PMC7048650.

29. Zhang Y. I-TASSER server for protein 3D structure prediction. BMC Bioinformatics. 2008; 9:40. Epub 2008/01/25. https://doi.org/10.1186/1471-2105-9-40 PMID: 18215316; PubMed Central PMCID: PMC2245901.

30. Roy A, Kucukural A, Zhang Y. I-TASSER: a unified platform for automated protein structure and function prediction. Nat Protoc. 2010; 5(4):725–38. Epub 2010/04/03. https://doi.org/10.1038/nprot.2010.5 PMID: 20360767; PubMed Central PMCID: PMC2849174.

31. Cheng J, Randall A, Baldi P. Prediction of protein stability changes for single-site mutations using support vector machines. Proteins. 2006; 62(4):1125–32. Epub 2005/12/24. https://doi.org/10.1002/prot.20810 PMID: 16372356.

32. Capriotti E, Fariselli P, Casadio R. I-Mutant2.0: predicting stability changes upon mutation from the protein sequence or structure. Nucleic Acids Res. 2005; 33(Web Server issue):W306–10. Epub 2005/06/28. https://doi.org/10.1093/nar/gki375 PMID: 15980478; PubMed Central PMCID: PMC1160136.

33. Chaudhary P, Naganathan AN, Gromiha MM. Folding RaCe: a robust method for predicting changes in protein folding rates upon point mutations. Bioinformatics. 2015; 31(13):2091–7. Epub 2015/02/18. https://doi.org/10.1093/bioinformatics/btv091 PMID: 25686635.

34. Rodrigues CH, Pires DE, Ascher DB. DynaMut: predicting the impact of mutations on protein conformation, flexibility and stability. Nucleic Acids Res. 2018; 46(W1):W350–W5. Epub 2018/05/03. https://doi.org/10.1093/nar/gky300 PMID: 29718330; PubMed Central PMCID: PMC6031064.

35. Anoosha P, Sakthivel R, Gromiha MM. Prediction of protein disorder on amino acid substitutions. Anal Biochem. 2015; 491:18–22. Epub 2015/09/09. https://doi.org/10.1016/j.ab.2015.08.028 PMID: 26348538.

36. Zhang Y, Wen Z, Washburn MP, Florens L. Refinements to label free proteome quantitation: how to deal with peptides shared by multiple proteins. Anal Chem. 2010; 82(6):2272–81. Epub 2010/02/20. https://doi.org/10.1021/ac9023999 PMID: 20166708.

37. Choi H, Kim S, Fermin D, Tsou CC, Nesvizhskii AI. QPROT: Statistical method for testing differential expression using protein-level intensity data in label-free quantitative proteomics. J Proteomics. 2015; 129:121–6. Epub 2015/08/09. https://doi.org/10.1016/j.jprot.2015.07.036 PMID: 26254008; PubMed Central PMCID: PMC4630079.

38. Hurst DR, Mehta A, Moore BP, Phadke PA, Meehan WJ, Accavitti MA, et al. Breast cancer metastasis suppressor 1 (BRMS1) is stabilized by the Hsp90 chaperone. Biochem Biophys Res Commun. 2006; 348(4):1429–35. Epub 2006/08/22. https://doi.org/10.1016/j.bbrc.2006.08.005 PMID: 16919237; PubMed Central PMCID: PMC1557677.

39. Hurst DR, Xie Y, Vaidya KS, Mehta A, Moore BP, Accavitti-Loper MA, et al. Alterations of BRMS1-ARID4A interaction modify gene expression but still suppress metastasis in human breast cancer cells. J Biol Chem. 2008; 283(12):7438–44. Epub 2008/01/24. https://doi.org/10.1074/jbc.M709446200 PMID: 18211900; PubMed Central PMCID: PMC2293288.

40. Chandrashekar DS, Bashel B, Balasubramanya SAH, Creighton CJ, Ponce-Rodriguez I, Chakravarthi B, et al. UALCAN: A Portal for Facilitating Tumor Subgroup Gene Expression and Survival Analyses. Neoplasia. 2017; 19(8):649–58. Epub 2017/07/22. https://doi.org/10.1016/j.neo.2017.05.002 PMID: 28732212; PubMed Central PMCID: PMC5516091.

41. Nagy A, Munkacsy G, Gyorffy B. Pancancer survival analysis of cancer hallmark genes. Sci Rep. 2021; 11(1):6047. Epub 2021/03/17. https://doi.org/10.1038/s41598-021-84787-5 PMID: 33723286; PubMed Central PMCID: PMC7961001.

42. Lai A, Kennedy BK, Barbie DA, Bertos NR, Yang XJ, Theberge MC, et al. RBP1 recruits the mSIN3-histone deacetylase complex to the pocket of retinoblastoma tumor suppressor family proteins found in limited discrete regions of the nucleus at growth arrest. Mol Cell Biol. 2001; 21(8):2918–32. Epub 2001/04/03. https://doi.org/10.1128/MCB.21.8.2918-2932.2001 PMID: 11283269; PubMed Central PMCID: PMC86920.

43. Suryadinata R, Sadowski M, Steel R, Sarcevic B. Cyclin-dependent kinase-mediated phosphorylation of RBP1 and pRb promotes their dissociation to mediate release of the SAP30.mSin3.HDAC transcriptional repressor complex. J Biol Chem. 2011; 286(7):5108–18. Epub 2010/12/15. https://doi.org/10.1074/jbc.M110.198473 PMID: 21148318; PubMed Central PMCID: PMC3037622.

44. Hein MY, Hubner NC, Poser I, Cox J, Nagaraj N, Toyoda Y, et al. A human interactome in three quantitative dimensions organized by stoichiometries and abundances. Cell. 2015; 163(3):712–23. Epub 2015/10/27. https://doi.org/10.1016/j.cell.2015.09.053 PMID: 26496610.

45. Fleischer TC, Yun UJ, Ayer DE. Identification and characterization of three new components of the mSin3A corepressor complex. Mol Cell Biol. 2003; 23(10):3456–67. Epub 2003/05/02. https://doi.org/10.1128/MCB.23.10.3456-3467.2003 PMID: 12724404; PubMed Central PMCID: PMC164750.

46. Marcon E, Ni Z, Pu S, Turinsky AL, Trimble SS, Olsen JB, et al. Human-chromatin-related protein interactions identify a demethylase complex required for chromosome segregation. Cell Rep. 2014; 8(1):297–310. Epub 2014/07/02. https://doi.org/10.1016/j.celrep.2014.05.050 PMID: 24981860.

47. Hsu DS, Wang HJ, Tai SK, Chou CH, Hsieh CH, Chiu PH, et al. Acetylation of snail modulates the cytokinome of cancer cells to enhance the recruitment of macrophages. Cancer Cell. 2014; 26(4):534–48. Epub 2014/10/15. https://doi.org/10.1016/j.ccell.2014.09.002 PMID: 25314079.

48. Laherty CD, Yang WM, Sun JM, Davie JR, Seto E, Eisenman RN. Histone deacetylases associated with the mSin3 corepressor mediate mad transcriptional repression. Cell. 1997; 89(3):349–56. Epub 1997/05/02. https://doi.org/10.1016/s0092-8674(00)80215-9 PMID: 9150134.

49. Tong JK, Hassig CA, Schnitzler GR, Kingston RE, Schreiber SL. Chromatin deacetylation by an ATP-dependent nucleosome remodelling complex. Nature. 1998; 395(6705):917–21. Epub 1998/11/06. https://doi.org/10.1038/27699 PMID: 9804427.

50. Joshi P, Greco TM, Guise AJ, Luo Y, Yu F, Nesvizhskii AI, et al. The functional interactome landscape of the human histone deacetylase family. Mol Syst Biol. 2013; 9:672. Epub 2013/06/12. https://doi.org/10.1038/msb.2013.26 PMID: 23752268; PubMed Central PMCID: PMC3964310.

51. Hassig CA, Fleischer TC, Billin AN, Schreiber SL, Ayer DE. Histone deacetylase activity is required for full transcriptional repression by mSin3A. Cell. 1997; 89(3):341–7. https://doi.org/10.1016/s0092-8674(00)80214-7 WOS:A1997WX89900004. PMID: 9150133

52. Skowyra D, Zeremski M, Neznanov N, Li M, Choi Y, Uesugi M, et al. Differential association of products of alternative transcripts of the candidate tumor suppressor ING1 with the mSin3/HDAC1 transcriptional corepressor complex. J Biol Chem. 2001; 276(12):8734–9. Epub 2000/12/29. https://doi.org/10.1074/jbc.M007664200 PMID: 11118440.

53. Hauri S, Comoglio F, Seimiya M, Gerstung M, Glatter T, Hansen K, et al. A High-Density Map for Navigating the Human Polycomb Complexome. Cell Rep. 2016; 17(2):583–95. Epub 2016/10/06. https://doi.org/10.1016/j.celrep.2016.08.096 PMID: 27705803.

54. Kuzmichev A, Zhang Y, Erdjument-Bromage H, Tempst P, Reinberg D. Role of the Sin3-histone deacetylase complex in growth regulation by the candidate tumor suppressor p33(ING1). Mol Cell Biol. 2002; 22(3):835–48. Epub 2002/01/11. https://doi.org/10.1128/MCB.22.3.835-848.2002 PMID: 11784859; PubMed Central PMCID: PMC133546.

55. Huttlin EL, Bruckner RJ, Paulo JA, Cannon JR, Ting L, Baltier K, et al. Architecture of the human interactome defines protein communities and disease networks. Nature. 2017; 545(7655):505–9. Epub 2017/05/18. https://doi.org/10.1038/nature22366 PMID: 28514442; PubMed Central PMCID: PMC5531611.

56. Nikolaev AY, Papanikolaou NA, Li M, Qin J, Gu W. Identification of a novel BRMS1-homologue protein p40 as a component of the mSin3A/p33(ING1b)/HDAC1 deacetylase complex. Biochem Biophys Res Commun. 2004; 323(4):1216–22. Epub 2004/09/29. https://doi.org/10.1016/j.bbrc.2004.08.227 PMID: 15451426.

57. Laherty CD, Billin AN, Lavinsky RM, Yochum GS, Bush AC, Sun JM, et al. SAP30, a component of the mSin3 corepressor complex involved in N-CoR-mediated repression by specific transcription factors. Mol Cell. 1998; 2(1):33–42. Epub 1998/08/14. https://doi.org/10.1016/s1097-2765(00)80111-2 PMID: 9702189

58. Zhang Y, Sun ZW, Iratni R, Erdjument-Bromage H, Tempst P, Hampsey M, et al. SAP30, a novel protein conserved between human and yeast, is a component of a histone deacetylase complex. Molecular Cell. 1998; 1(7):1021–31. https://doi.org/10.1016/s1097-2765(00)80102-1 WOS:000074389200009. PMID: 9651585

59. Hurst DR, Welch DR. Unraveling the enigmatic complexities of BRMS1-mediated metastasis suppression. FEBS Lett. 2011; 585(20):3185–90. Epub 2011/08/11. https://doi.org/10.1016/j.febslet.2011.07.045 PMID: 21827753; PubMed Central PMCID: PMC3195837.

60. Koyama R, Tamura M, Nakagaki T, Ohashi T, Idogawa M, Suzuki H, et al. Identification and characterization of a metastatic suppressor BRMS1L as a target gene of p53. Cancer Sci. 2017; 108(12):2413–21. Epub 2017/10/17. https://doi.org/10.1111/cas.13420 PMID: 29030916; PubMed Central PMCID: PMC5715288.

61. Gong C, Qu S, Lv XB, Liu B, Tan W, Nie Y, et al. BRMS1L suppresses breast cancer metastasis by inducing epigenetic silence of FZD10. Nat Commun. 2014; 5:5406. Epub 2014/11/20. https://doi.org/10.1038/ncomms6406 PMID: 25406648.

62. Mellacheruvu D, Wright Z, Couzens AL, Lambert JP, St-Denis NA, Li T, et al. The CRAPome: a contaminant repository for affinity purification-mass spectrometry data. Nat Methods. 2013; 10(8):730–6. Epub 2013/08/08. https://doi.org/10.1038/nmeth.2557 PMID: 23921808; PubMed Central PMCID: PMC3773500.

63. Hicks DG, Janarthanan BR, Vardarajan R, Kulkarni SA, Khoury T, Dim D, et al. The expression of TRMT2A, a novel cell cycle regulated protein, identifies a subset of breast cancer patients with HER2 over-expression that are at an increased risk of recurrence. BMC Cancer. 2010; 10:108. Epub 2010/03/24. https://doi.org/10.1186/1471-2407-10-108 PMID: 20307320; PubMed Central PMCID: PMC2859753.

64. Chen C, Zhou Z, Ross JS, Zhou W, Dong JT. The amplified WWP1 gene is a potential molecular target in breast cancer. Int J Cancer. 2007; 121(1):80–7. Epub 2007/03/03. https://doi.org/10.1002/ijc.22653 PMID: 17330240.

65. Gkountela S, Castro-Giner F, Szczerba BM, Vetter M, Landin J, Scherrer R, et al. Circulating Tumor Cell Clustering Shapes DNA Methylation to Enable Metastasis Seeding. Cell. 2019; 176(1–2):98–112.e14. Epub 2019/01/12. https://doi.org/10.1016/j.cell.2018.11.046 PMID: 30633912; PubMed Central PMCID: PMC6363966.

66. Buchner A, Castro M, Hennig A, Popp T, Assmann G, Stief CG, et al. Downregulation of HNF-1B in renal cell carcinoma is associated with tumor progression and poor prognosis. Urology. 2010; 76(2):507e6-11. Epub 2010/06/12. https://doi.org/10.1016/j.urology.2010.03.042 PMID: 20538322.

67. Frayling TM, Colhoun H, Florez JC. A genetic link between type 2 diabetes and prostate cancer. Diabetologia. 2008; 51(10):1757–60. Epub 2008/08/13. https://doi.org/10.1007/s00125-008-1114-9 PMID: 18696045.

68. Champine PJ, Michaelson J, Weimer BC, Welch DR, DeWald DB. Microarray analysis reveals potential mechanisms of *BRMS1*-mediated metastasis suppression. Clin Exp Metastasis. 2007; 24(7):551–65. Epub 2007/09/27. https://doi.org/10.1007/s10585-007-9092-8 PMID: 17896182; PubMed Central PMCID: PMC2214901.

69. Mei P, Bai J, Shi M, Liu Q, Li Z, Fan Y, et al. BRMS1 suppresses glioma progression by regulating invasion, migration and adhesion of glioma cells. PLoS One. 2014; 9(5):e98544. Epub 2014/06/01. https://doi.org/10.1371/journal.pone.0098544 PMID: 24879377; PubMed Central PMCID: PMC4039505.

70. Khotskaya YB, Beck BH, Hurst DR, Han Z, Xia W, Hung MC, et al. Expression of metastasis suppressor BRMS1 in breast cancer cells results in a marked delay in cellular adhesion to matrix. Mol Carcinog. 2014; 53(12):1011–26. Epub 2013/09/04. https://doi.org/10.1002/mc.22068 PMID: 24000122; PubMed Central PMCID: PMC3939074.

71. Shevde LA, Samant RS, Goldberg SF, Sikaneta T, Alessandrini A, Donahue HJ, et al. Suppression of human melanoma metastasis by the metastasis suppressor gene, BRMS1. Exp Cell Res. 2002; 273 (2):229–39. Epub 2002/02/02. https://doi.org/10.1006/excr.2001.5452 PMID: 11822878.

72. Friedl P, Hegerfeldt Y, Tusch M. Collective cell migration in morphogenesis and cancer. Int J Dev Biol. 2004; 48(5–6):441–9. Epub 2004/09/07. https://doi.org/10.1387/ijdb.041821pf PMID: 15349818.

73. Zhang HM, Qiao QD, Xie HF, Wei JX. Breast cancer metastasis suppressor 1 (BRMS1) suppresses prostate cancer progression by inducing apoptosis and regulating invasion. Eur Rev Med Pharmacol Sci. 2017; 21(1):68–75. Epub 2017/01/26. PMID: 28121354.

74. Liu Y, Smith PW, Jones DR. Breast cancer metastasis suppressor 1 functions as a corepressor by enhancing histone deacetylase 1-mediated deacetylation of RelA/p65 and promoting apoptosis. Mol Cell Biol. 2006; 26(23):8683–96. Epub 2006/09/27. https://doi.org/10.1128/MCB.00940-06 PMID: 17000776; PubMed Central PMCID: PMC1636810.

75. Smith PW, Liu Y, Siefert SA, Moskaluk CA, Petroni GR, Jones DR. Breast cancer metastasis suppressor 1 (BRMS1) suppresses metastasis and correlates with improved patient survival in non-small cell lung cancer. Cancer Lett. 2009; 276(2):196–203. Epub 2008/12/30. https://doi.org/10.1016/j.canlet.2008.11.024 PMID: 19111386; PubMed Central PMCID: PMC4793277.

76. Hurst DR, Edmonds MD, Welch DR. Metastamir: the field of metastasis-regulatory microRNA is spreading. Cancer Res. 2009; 69(19):7495–8. Epub 2009/09/24. https://doi.org/10.1158/0008-5472.CAN-09-2111 PMID: 19773429; PubMed Central PMCID: PMC2756311.

77. Hedley BD, Welch DR, Allan AL, Al-Katib W, Dales DW, Postenka CO, et al. Downregulation of osteopontin contributes to metastasis suppression by breast cancer metastasis suppressor 1. Int J Cancer. 2008; 123(3):526–34. Epub 2008/05/13. https://doi.org/10.1002/ijc.23542 PMID: 18470911.

78. DeWald DB, Torabinejad J, Samant RS, Johnston D, Erin N, Shope JC, et al. Metastasis suppression by breast cancer metastasis suppressor 1 involves reduction of phosphoinositide signaling in MDA-MB-435 breast carcinoma cells. Cancer Res. 2005; 65(3):713–7. Epub 2005/02/12. PMID: 15705865.

79. Ma L, Teruya-Feldstein J, Weinberg RA. Tumour invasion and metastasis initiated by microRNA-10b in breast cancer. Nature. 2007; 449(7163):682–8. Epub 2007/09/28. https://doi.org/10.1038/nature06174 PMID: 17898713.

80. McDonel P, Demmers J, Tan DW, Watt F, Hendrich BD. Sin3a is essential for the genome integrity and viability of pluripotent cells. Developmental biology. 2012; 363(1):62–73. Epub 2011/12/31. https://doi.org/10.1016/j.ydbio.2011.12.019 PMID: 22206758; PubMed Central PMCID: PMC3334623.

81. Gerami P, Cook RW, Wilkinson J, Russell MC, Dhillon N, Amaria RN, et al. Development of a prognostic genetic signature to predict the metastatic risk associated with cutaneous melanoma. Clin Cancer Res. 2015; 21(1):175–83. Epub 2015/01/08. https://doi.org/10.1158/1078-0432.CCR-13-3316 PMID: 25564571.